Evaluation of Unsteady Pressure Sensitive Paint Measurement Technique for Space Launch Vehicle Buffet Determination

Marvin E. Sellers[1] and Michael A. Nelson[2]
Quantitech, Arnold AFB, TN, 37389

Nettie H. Roozeboom[3] and Nathan J. Burnside[4]
NASA Ames Research Center, Moffett Field, CA, 94035

Launch vehicle buffet loads have been determined by using unsteady pressure transducers that measure pressure fluctuations at several hundred locations on a wind tunnel model and then integrating the pressure fluctuations over a specified area. Even with this very large number of sensors, the coverage is insufficient to provide accurate integrated unsteady loads on the vehicle and the coarse spacing of the sensors results in buffet environments that are often conservative in their prediction of buffet loads between the transducers. This results in additional structural weight to cover these conservative environments. Computational fluid dynamics (CFD) is potentially capable of modeling these environments but is currently too slow and not well validated for unsteady loads. NASA and the aerospace industry need a defendable, reliable method to estimate buffet forcing functions (BFF) from the limited unsteady pressure data that is available from wind-tunnel testing and to instill confidence in CFD techniques to obtain the same information. Recently, AEDC has begun development of an unsteady pressure sensitive paint (uPSP) capability for 16T that can acquire fluctuating pressures up to 20 kHz and has demonstrated a prototype on a generic weapons bay model. The excellent results from that test encouraged NASA Ames to request uPSP support for a launch vehicle buffet verification test in their 11-foot wind tunnel. A wind tunnel model identical in configuration to Model 11 tested by Coe and Nute was designed for the test. In addition to the conventional unsteady pressure transducers and static pressure orifices, the model would be covered with uPSP to measure full surface fluctuating pressures. A 12.1-inch section of the second stage was instrumented with gages and accelerometers in hopes of directly measuring fluctuating loads. Verification of the uPSP is made through power spectral density (PSD) comparisons with conventional unsteady pressure transducers and comparisons of fluctuating section load integrations from PSP and transducers at each section (PSD and RMS loads). Additionally, the uPSP data quality is verified via auto correlation between cameras in overlap regions. The complete spatial distribution of the sound pressure level (SPL) at selected frequencies and RMS is presented to aid understanding of the data and provide additional insight. The continuous uPSP illustrates the small coherence distance that is valid for conventional transducers to be applied in calculating unsteady forces, whereas the uPSP is not bound by this limitation. Analysis of the buffet forcing functions will be presented as RMS section loads (per unit length). The results of the test demonstrate the ability to determine more accurate buffet forcing functions using unsteady PSP than is possible with sparse point source instrumentation.

---

[*] *The research reported herein was performed by the Arnold Engineering Development Complex (AEDC), Air Force Materiel Command. Work and analysis for this research were performed by personnel of Quantitech, a support contractor for AEDC. Further reproduction is authorized to satisfy needs of the U. S. Government.*

[1]*AEDC Fellow, Integrated Test & Evaluation, Flight Systems, 740 Fourth St, MS6001.*
[2]*PSP Engineer, Integrated Test & Evaluation, Flight Systems, 740 Fourth St, MS6001*
[3]*Aerospace Engineer, Experimental Aero-Physics Branch, M.S. 260-1*
[4]*Aerospace Engineer, Experimental Aero-Physics Branch, M.S. 260-1*

Nomenclature

AF	=	axial force per unit length, lb/in.
Alpha	=	model angle of attack, deg
Beta	=	model sideslip angle, deg
CONFIG	=	configuration designation number
f	=	frequency, Hz
FFT	=	fast-Fourier transform
Gain	=	gain conversion factor, psi/(intensity ratio)
I	=	paint luminescence intensity at pressure
Kxx-yy	=	Kulite® transducer identification, where xx is station and yy is radial number
LED	=	light-emitting diode
Mach, M	=	freestream Mach number
NF	=	normal force per unit length, lb/in.
P	=	pressure at wind-on condition, psfa
Prms	=	uPSP RMS pressure, psi
PSD	=	power spectral density, psi^2/Hz or (lb/in.)^2/Hz
Q	=	dynamic pressure, psf
r	=	temperature recovery factor (see Eq. 2)
RMS	=	root-mean-square
T	=	PSP calibration or model surface temperature, ºF
T_∞	=	free-stream temperature, ºF
TT	=	tunnel stagnation temperature, ºF
uPSP	=	unsteady pressure-sensitive paint
SF	=	side force per unit length, lb/in.
SPL	=	sound pressure level, dB
Sta.	=	model station, in.
t	=	time, s

I. Introduction

LAUNCH vehicle buffet loads have been determined by using unsteady pressure transducers that measure pressure fluctuations at several hundred locations on a wind tunnel model and then integrating the pressure fluctuations over a specified area. Even with this very large number of sensors, the coverage is insufficient to provide accurate integrated unsteady loads on the vehicle and the coarse spacing of the sensors results in buffet environments that are often conservative in their prediction of buffet loads between the transducers. This results in additional structural weight to cover these conservative environments. Computational fluid dynamics (CFD) is potentially capable of modeling these environments but is currently too slow and not well validated for unsteady loads. NASA and the aerospace industry need a defendable, reliable method to estimate buffet forcing function (BFF) from the limited unsteady pressure data that is available from wind-tunnel testing and to instill confidence in CFD techniques to obtain the same information.

Engineers at the Arnold Engineering Development Complex (AEDC) have utilized a steady-state pressure-sensitive paint (PSP) capability in Propulsion Wind Tunnel (PWT) 16T to acquire surface pressure data on wind tunnel models (Refs. 1-10). NASA Ames has implemented the same system in the 11-foot and 9x7 tunnels. Recently, AEDC has begun development of an unsteady PSP (uPSP) capability for 16T that can acquire fluctuating pressures up to 20 kHz and has demonstrated a prototype on a generic weapons bay model (Ref. 11). Some advantages of using PSP are 1) it provides a continuous pressure distribution, 2) it permits the acquisition of data in areas inaccessible to conventional pressure measurements, and 3) it provides data mapped to a 3-D surface grid similar to CFD, permitting better validation of CFD results. In addition, PSP data can easily be integrated over individual surfaces to determine panel loads and provide a better integration. NASA Ames requested AEDC to provide uPSP support for a launch vehicle buffet verification test in their 11-foot wind tunnel. A wind tunnel model identical in configuration to Model 11 tested by Coe and Nute (Ref. 12) was designed for the test. In addition to the conventional unsteady pressure transducers and static pressure orifices, the model was covered with uPSP to measure full surface fluctuating pressures. A 12.1-in. section of the second stage was instrumented with gages and accelerometers in hopes of directly measuring fluctuating loads. Verification of the uPSP will be made through power spectral density (PSD) comparisons with conventional unsteady pressure transducers and comparisons of fluctuating section load integrations from PSP and transducers at each section. Additionally, the uPSP data quality is verified via auto correlation between cameras in overlap regions. The complete spatial distribution of the sound pressure level (SPL) at selected frequencies and RMS is presented to aid understanding of the data and provide additional insight. Analysis of the buffet forcing functions will be presented as RMS section loads (per unit length).

II. Background

A. Pressure-Sensitive Paint

The uPSP selected for the test was polymer-ceramic PSP, from Innovative Scientific Solutions, Inc. (ISSI), because it can detect pressure fluctuations up to 20 kHz. The pressure sensitive component of the paint was platinum tetra (pentafluorophenyl) porphyrin (PtTFPP). Details of the paint can be found in work by Gregory *et al.* (Ref. 13) and Flaherty *et al.* (Ref. 14). The details of the uPSP application and data acquisition are covered in Sellers *et al.* (Ref. 11) and will be addressed in a limited fashion in order to focus on the results of the test.

III. Test Setup

A. Test Article

The test article was a scale model of a generic launch vehicle (Model 11) from Coe and Nute with a 12-in. maximum diameter. The model was instrumented with 211 Kulite® dynamic pressure transducers and 121 static pressure taps. In addition, a 12.1-in. long section of the second stage was instrumented to measure normal and side load fluctuations. Details of the test article are presented in Fig. 1 along with a pictorial distribution of the Kulites. The section locations (Kxx) of the Kulites and the number of transducers at each station are presented in Fig. 2. The two stations with 16V have transducers concentrated radially on the top surface. Two flanges were available to add to the downstream end of the second stage to evaluate their effect on the local aeroacoustic environment. The three configurations tested were baseline (no flanges) and 1 or 2 flanges added.

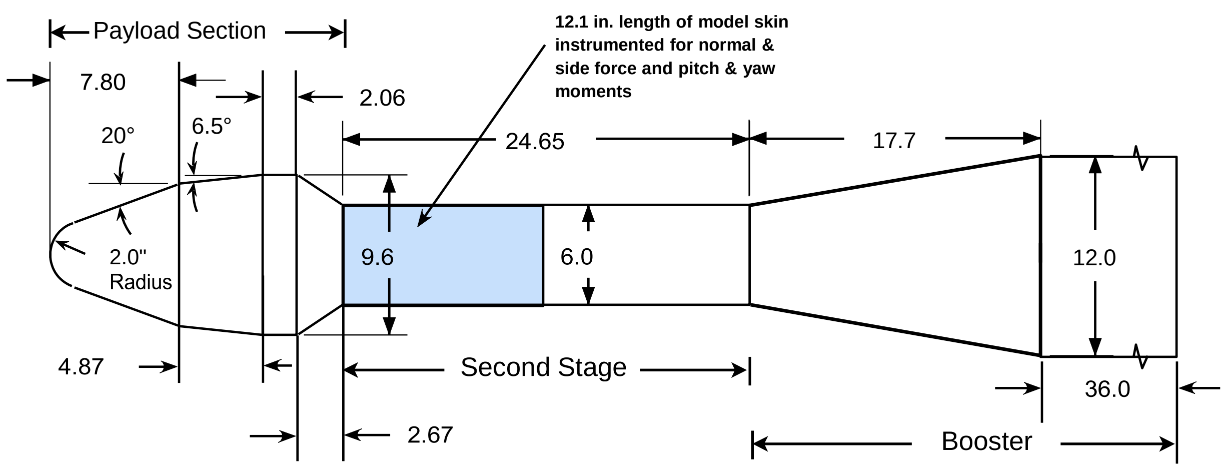

a. Dimensions, inches.

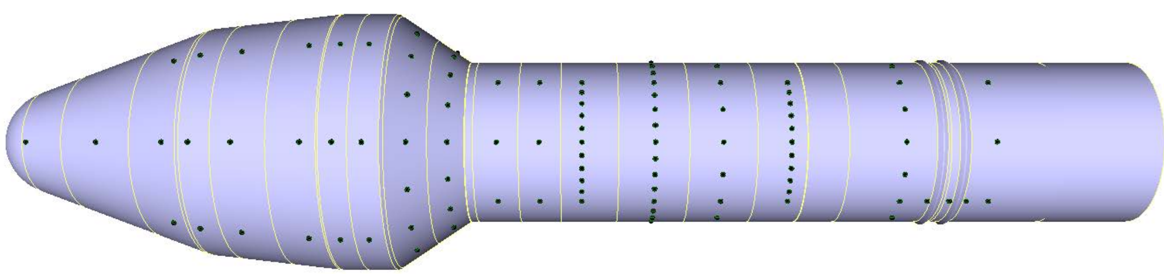

b. Kulite pictorial distribution, top view.
Figure 1. Test article details.

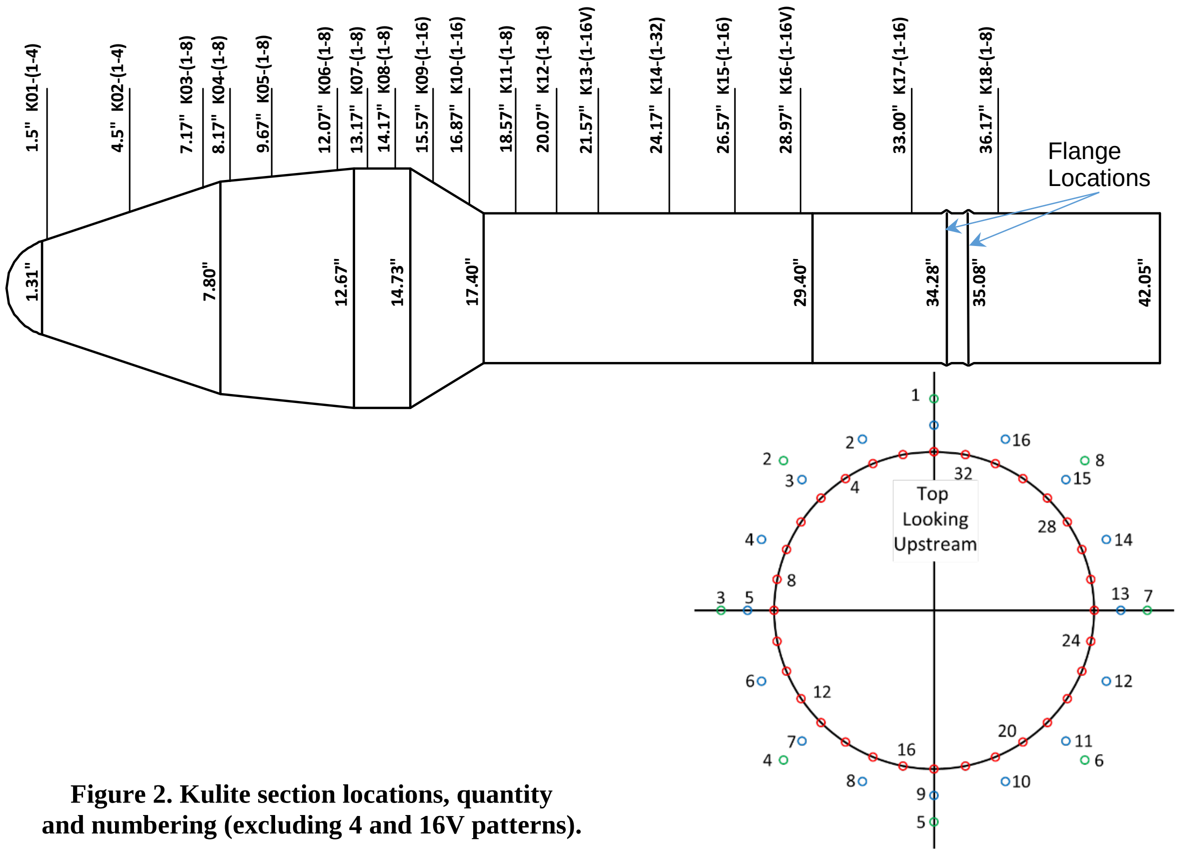

Figure 2. Kulite section locations, quantity and numbering (excluding 4 and 16V patterns).

B. Data Acquisition

The uPSP on the test article was imaged using four Vision Research Phantom® v1211 high-speed cameras at speeds of 5000, 10000, and 20000 frames/sec. An AEDC prototype uPSP data acquisition system was used to control and acquire data from the high speed cameras. In addition, the NASA Ames lifetime PSP system was utilized to measure the steady-state pressure distribution over the model surface. This system used eight Photometrics® CoolSnap K4 cameras to capture images of the PSP fluorescence. The uPSP was excited with 40 ISSI 400nm LED units for both steady-state and unsteady systems. The LEDs operated in pulsed mode for the steady-state system and in continuous mode for the unsteady system. The data acquisition sequence was set up to first acquire conventional steady-state pressures, using Electronically Scanned Pressure (ESP) transducers, and steady-state PSP data. Next, the unsteady pressure transducers, balance, accelerometer, and uPSP data were acquired. The facility unsteady data acquisition system and the uPSP data system were not synchronized in time and recorded at different sample rates (except for the 10000 frame/sec rate). The facility unsteady data acquisition system acquired data at dual rates of 10k and 100k samples/sec. For the majority of the test, 62000 image frames were acquired from each Phantom camera. Approximately 130GB of uPSP data were acquired for each data point with a total of 14TB acquired for the test which consisted of 114 data points. Actual clock time of uPSP acquisition to generate this volume of data was just under six minutes for the test.

C. Data Reduction

The standard image processing approach for lifetime PSP (Refs. 6-10) was used for the steady-state PSP data. The uPSP data were processed in AC fashion (i.e. intensity fluctuations relative to the average) using the intensity ratio technique, I_{ref}/I. The reference image was computed from the average of all frames and the intensity ratio by dividing each frame into the reference and subtracting 1. The result for each frame was converted to pressure using the following equation:

$$P = \left(I_{ref}/I - 1\right) * \left(Gain\right) \quad (1)$$

where *Gain* was determined from a steady-state, intensity ratio calibration of a uPSP sample. The intensity ratio calibration of the uPSP over two pressure ranges are presented in Fig. 3.

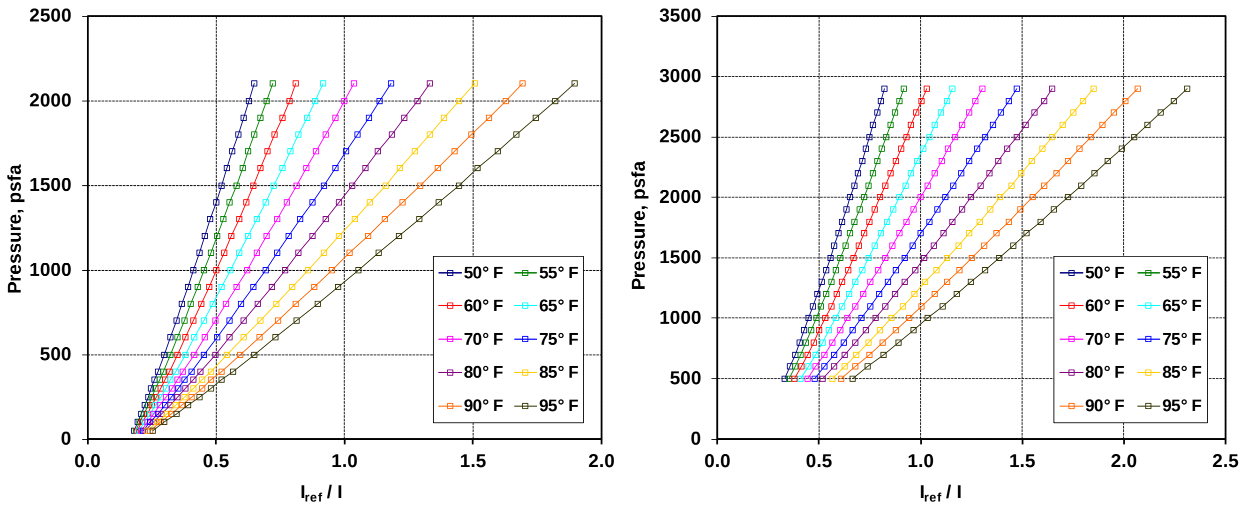

a. Low pressure range. **b. High pressure range.**

Figure 3. Intensity ratio calibration.

Gain is the local slope of the intensity ratio calibration at each pressure and temperature and the gain calibration curves for the two pressure ranges are presented in Fig. 4. Evident in the plots is a strong sensitivity to temperature and the fact that the absolute pressure is required to determine the gain. The lifetime PSP system (using a lifetime PSP calibration, not shown) was used to acquire the absolute pressure (*P*) and the model surface temperature (*T*) was estimated using the turbulent boundary-layer recovery factor of 0.896 given by Schlichting (Ref. 15) and the following equation:

$$T = r\,(TT - T_{\infty}) + T_{\infty} \tag{2}$$

Gain was calculated from the calibration using the following equation:

$$Gain = a + bT + cT^2 + (d + eT + fT^2) * (P) \tag{3}$$

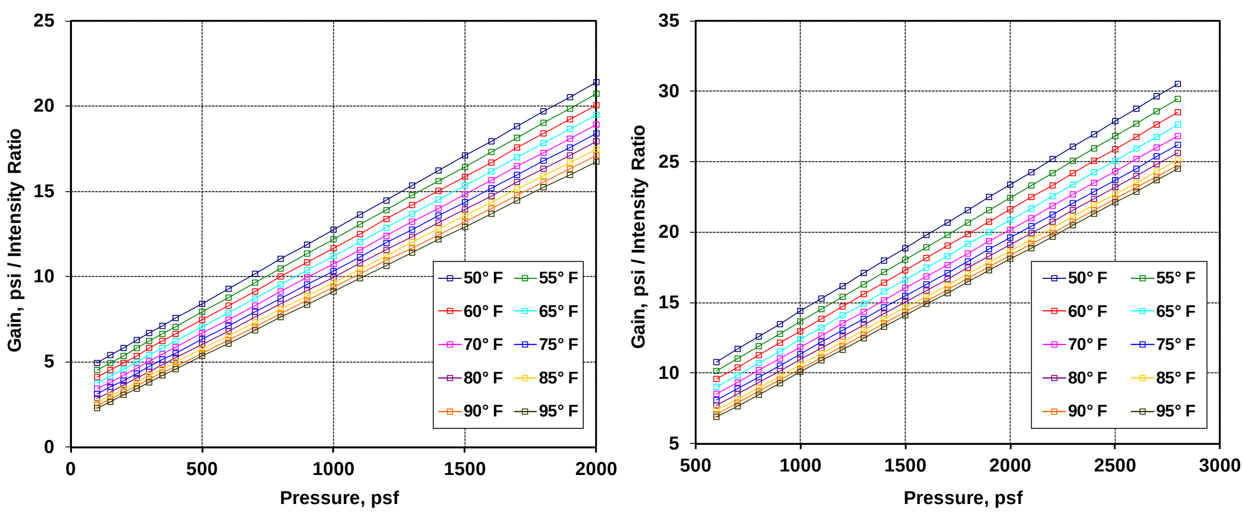

a. Low pressure range. **b. High pressure range.**

Figure 4. Gain calibration curves.

A 3-D time history file was generated for each uPSP data point with pressure data in psi at each vertex point in the model grid. In addition, time history fluctuating forces and moments in lb and in.-lb were computed along the model at 77 locations, from Sta. 1.316 to 38.0, and normalized by the length of integration (approximately 0.5 in.). The uPSP time history data were detrended and filtered with a two-pass (forward and backward), 4^{th}-order Butterworth filter at a cutoff frequency of 80% of the Nyquist frequency.

The 10k unsteady transducer data was detrended and filtered with a two-pass 4^{th}-order Butterworth and 2000 Hz cut-off for the decimated 5000 samples/sec rate and 8000 Hz cut-off for the 10000 samples/sec rate. The 100k unsteady transducer data was detrended and filtered with a two-pass 16^{th}-order Butterworth and 16000 Hz cut-off for the decimated 20000 samples/sec rate. The primary reason for the strong filtering was to approximately obtain the same roll-off rate at the cut-off frequency of the uPSP to enable equivalent RMS comparisons. The Kulites at each station were integrated to generate time history normalized fluctuating forces (lb/in.). Bad Kulites were substituted with the average of the nearest two Kulites (azimuthally). The arc length over which the Kulite data was integrated was dependent on the number of transducers at each station. The asymmetric transducers at the 16V stations were not included in the integration.

Comparisons of time history data between the unsteady pressure transducers and PSP are not possible since they were recorded by systems not synchronized in time. However, comparisons of data in the frequency domain can be made. The two sets of data were processed identically to produce the PSD data at the transducer locations. The PSD was calculated using an ensemble size of 4096, with 50% overlap, and a Hanning window. The Hanning window was calculated using

$$window(i+1) = 2.0*(0.5-0.5*\cos((2\pi/4096)*i)),\ \ where\ i=0\ to\ 4095 \tag{4}$$

and applied to each ensemble prior to calculating the FFT amplitude. The spectral leakage (Ref. 16) of the Hanning window is accounted for by dividing by 1.5 for PSD and square root of 1.5 for SPL. The resulting averaged amplitude of the FFT was converted to PSD (psi^2/Hz or (lb/in.)^2/Hz) using

$$PSD(i) = (amplitude\ (i)^{\,2} * 4096/sample\_rate)/2/1.5,\ \ where\ i=1\ to\ 2047 \tag{5}$$

and frequency values were defined as

$$f\,(i) = (sample\_rate\ /4096)*i\ ,\ \ where\ i=1\ to\ 2047 \tag{6}$$

The sound pressure level (SPL) in decibel (dB) was calculated using

$$SPL(i) = 20*\log10(amplitude(i)/2.90075e-9/\sqrt{1.5}),\ \ where\ i=1\ to\ 2047 \tag{7}$$

For the 3-D continuous distribution of PSP, the RMS and SPL of the pressure fluctuation was calculated at every vertex that had valid data. A modified PLOT3D file was generated for each data point with SPL level at each vertex for every frequency in the bin. Sound pressure level was used to enhance data visualization. The standard PLOT3D format used for steady-state PSP was also used for the RMS (psi) distribution for each data point. A special PSP viewer was developed to permit stepping through the frequencies and visualizing the SPL distribution in 3-D. To enable PSD plot comparisons of the unsteady pressure transducer and the uPSP data, uPSP data were extracted from the 3-D files at corresponding locations of the transducers. Although there was no PSP on the transducers, data surrounding the transducers were used to interpolate over the missing paint.

IV. Experimental Results

A. Unsteady Pressure Measurement Comparisons

The validation of the uPSP results will begin with comparisons of PSDs from the unsteady pressure transducers and uPSP. It is difficult to present the vast amount of comparisons that can be made, i.e. every transducer location vs. uPSP for every data point, therefore a sampling representative of the test will be presented. The majority of the test was conducted at Reynolds number 3 million/ft with a limited amount of data acquired at 2 and 5 million/ft. The data presented in this paper are for Reynolds number 3 million/ft and 5 kHz sample rate unless otherwise stated. A condition with the largest differences, Mach 0.6, is presented in Fig. 5 for stations 3-17. The comparison at stations 3-7 have significant differences and are the result of small pressure fluctuation magnitudes that the Kulites can easily detect but are below the noise floor of uPSP. Peaks present in the uPSP data (~22 Hz and harmonics) and not the Kulite data are the result of camera 2 movement (left side of model, looking upstream). Movement of the model or cameras will be perceived as a pressure fluctuation, even though each image is shifted at sub-pixel level before computing the intensity ratio. This was verified by analyzing the registration target movement with time and computing the frequency of the movement. Stations 8-15 have much better agreement where the pressure fluctuations are more significant. The noise floor appears to be a magnitude of 10^{-6} at this condition and is evident at frequencies above 500 Hz when the Kulite data falls below this level. It is difficult to see, but the uPSP matches the peaks of the Kulites for frequencies above 100 Hz when the level is above the uPSP noise floor. The two peaks at 345 and 690 Hz are present in empty tunnel data and are generated by the drive system. The tunnel noise is eventually masked by aerodynamic noise generated by the model at stations on the second stage.

A comparison with some of the best results is presented in Fig. 6 for Mach 0.85, which had more energy content as the result of non-stationary shock waves adjacent to the expansion corners. Stations 3, 4, and 6 still have significant differences but stations 5 and 7 have better agreement as the result of the fluctuating shocks which resulted in high pressure fluctuations. The strong 7 Hz peak at station 5 has excellent agreement between uPSP and Kulites. The comparison for stations 8-17 are also much better at this condition. Two drive tones at 400 and 510 Hz were present in the data when the model-generated noise was small. A comparison of Kulite and uPSP data at 5 kHz (Run 17001) and 10 kHz (Run 17601) sample rate is presented in Fig. 7 for one sensor location. Another significant peak detected by the Kulite and PSP in the 10 kHz data occurs at approximately 3000 Hz and is also a dominant tone in the empty tunnel data. It is possible the content at this frequency folded over in the 5 kHz PSP data and is part of the reason for disagreement between the two PSP rates. Also note the PSP noise floor does not appear to have been reached with agreement down to 10^{-7} with the Kulite data. No explanation has been discovered for the peak at 2300 Hz in the 10 kHz uPSP data (not present in the Kulite data).

In order to gain an understanding of the comparisons between uPSP and Kulite data, the correlation coefficient between uPSP data from two cameras was computed. Approximately 40 deg of overlap on the surface grid existed between cameras, so correlations were computed between cameras 1&2, 2&3, 3&4, and 4&1 in these regions. The correlation coefficient distribution is presented in Fig. 8 for each Mach number with the model at Alpha -4 deg. When the correlation was less than 0.2 the uPSP was dominated by noise and these regions correspond with large disagreement between the uPSP and the Kulites. The noise on the nose and at the end of the second stage results from small intensity fluctuations (relative to the 10-bit dynamic range of the camera). As the correlation coefficient increased, the agreement with the Kulites improved until the best agreement was reached in areas with a coefficient near 1. Notice the high correlation regions near station 5 and 7 (Fig. 8c) where fluctuating shocks were present. A by-product of the correlation was the phase information which indicated no time delay between the cameras, as expected, in areas with high correlation. Of course, if part of the image is fully in phase, the whole image is in phase.

The RMS distribution of the fluctuating pressure is presented in Fig. 9 along with the Kulite values as colored bubbles for comparison with the uPSP. The black colored bubbles are locations with bad transducers. The uPSP RMS values are larger than the Kulite data on the nose of the payload, as expected since the uPSP was dominated by noise. The majority of the Kulites on the boattail and second stage agree much better with the uPSP, as do the Kulites on the nose when a shock was on their location. The standing shocks and separated flow reattachment regions are visible in these images.

A consideration was given to using the RMS values from the transducers to adjust the PSP data via *in-situ* calculation of a distributed gain adjustment. The difference between uPSP and transducer RMS was computed at each location and a 3-D distribution technique was applied to calculate a gain adjustment at each vertex of the grid. As expected, the PSD comparisons improved in most areas (even the noise limited region) but made the comparison worse at stations 5 and 7 for Mach 0.85. The distribution of gain adjustment smoothed over the sharp increase in RMS at the shock locations and resulted in a reduction of the uPSP magnitude. The technique was determined to produce false agreement and therefore was not implemented.

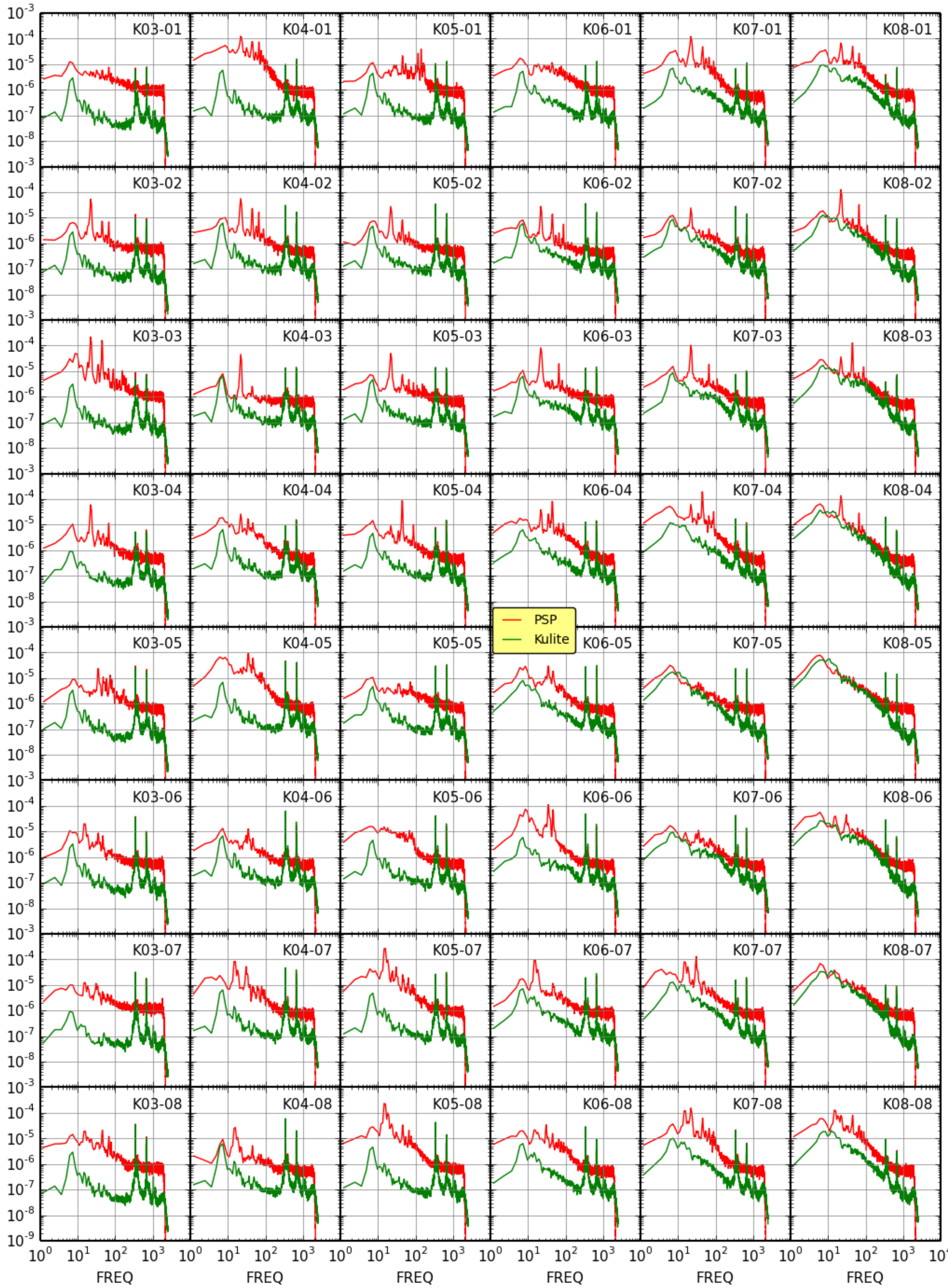

a. Stations 3 through 8.
Figure 5. PSD (psi²/Hz) comparison, Mach 0.6, Alpha -4 deg.

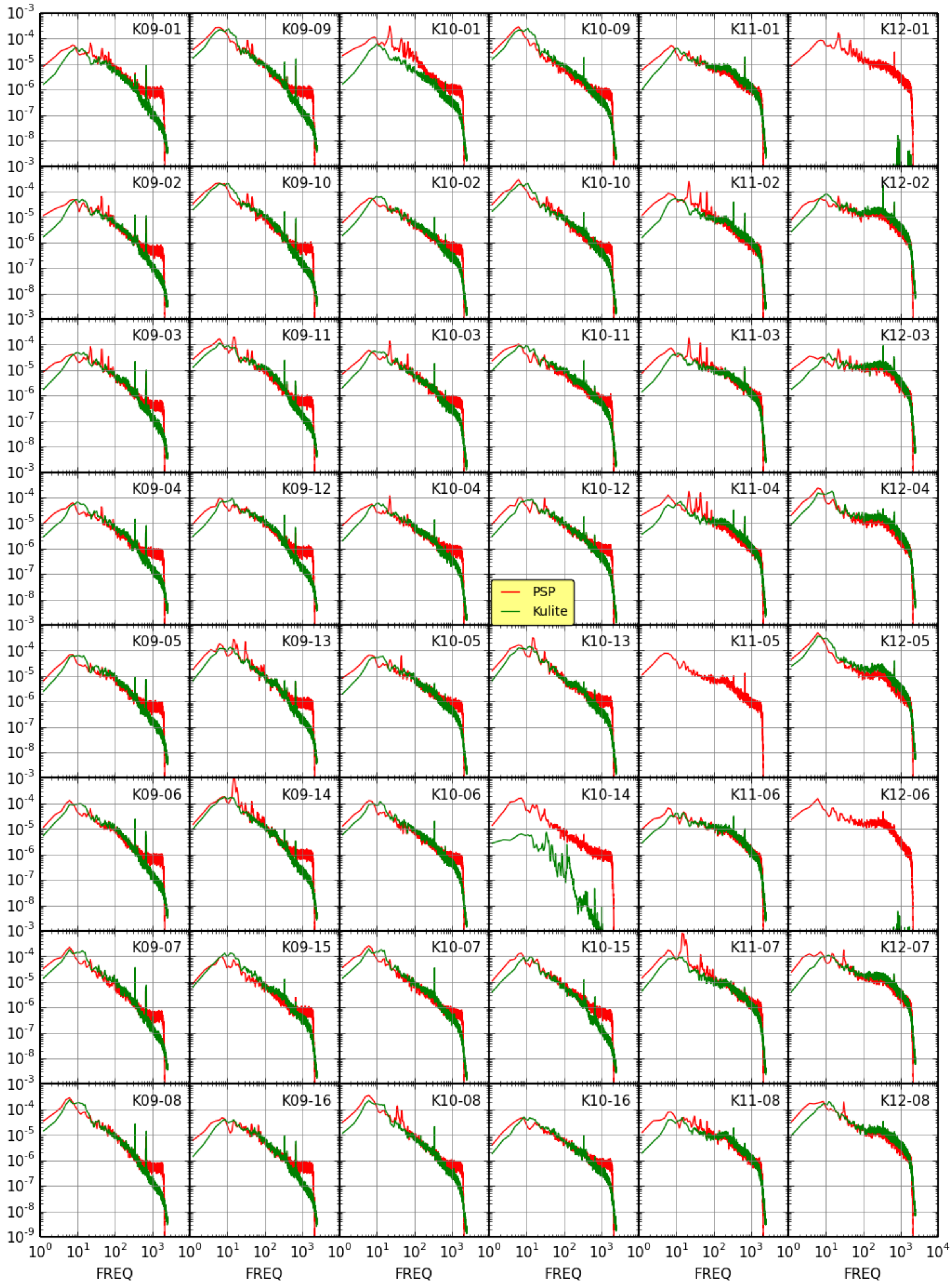

b. Stations 9 through 12.
Figure 5. Continued.

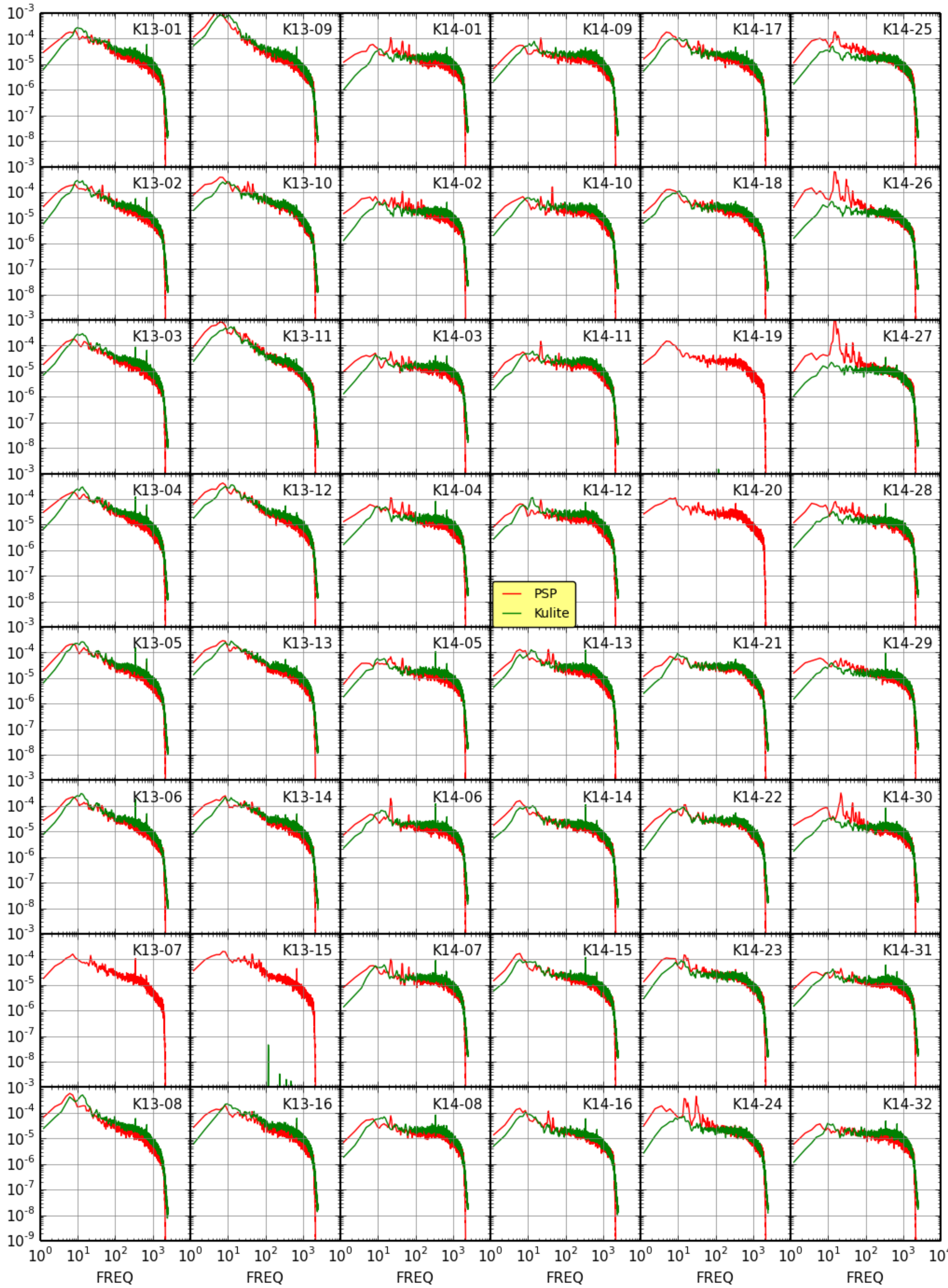

c. Stations 13 through 14.
Figure 5. Continued.

Approved for public release; distribution is unlimited.

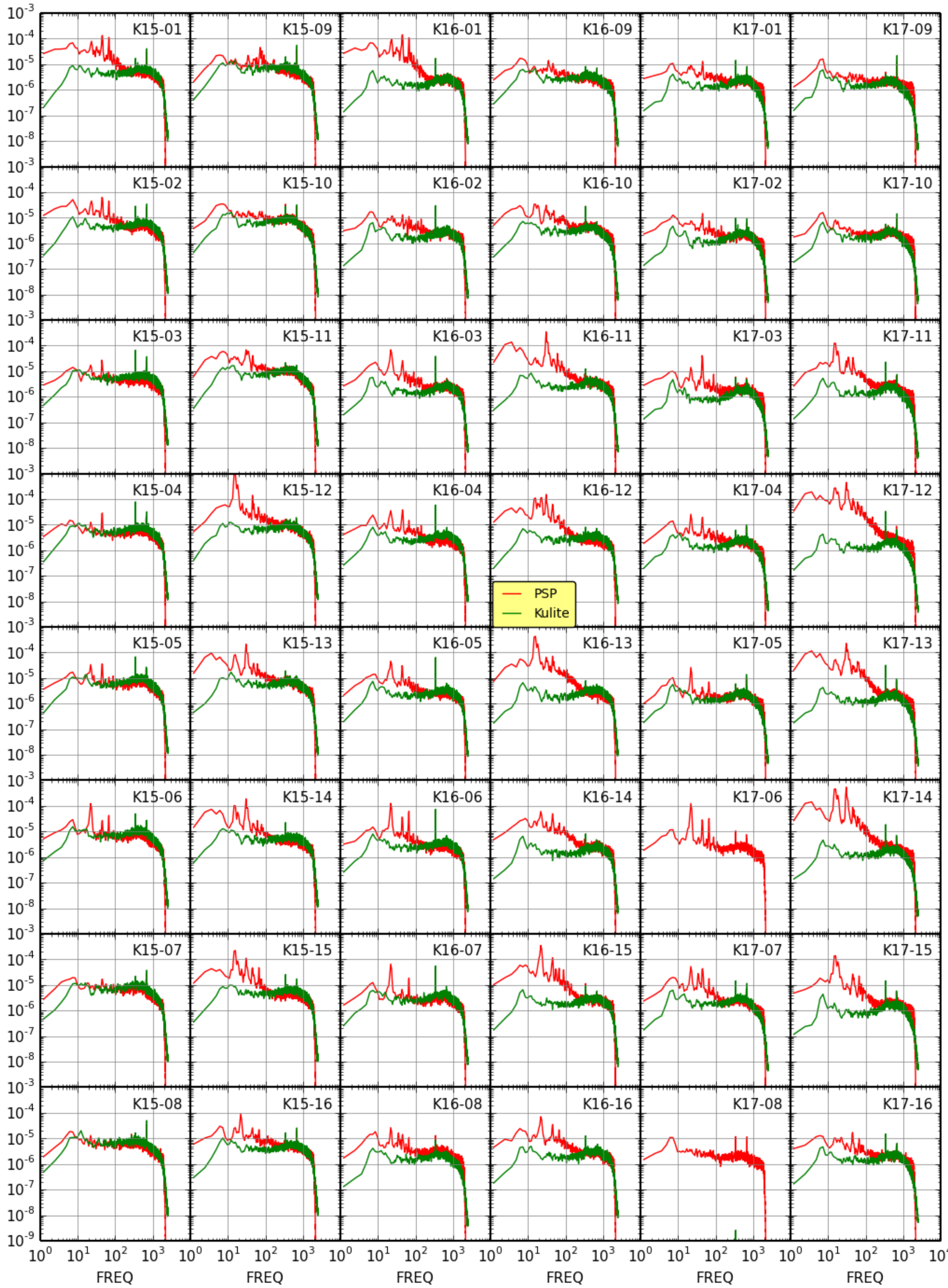

d. Stations 15 through 17.
Figure 5. Concluded.

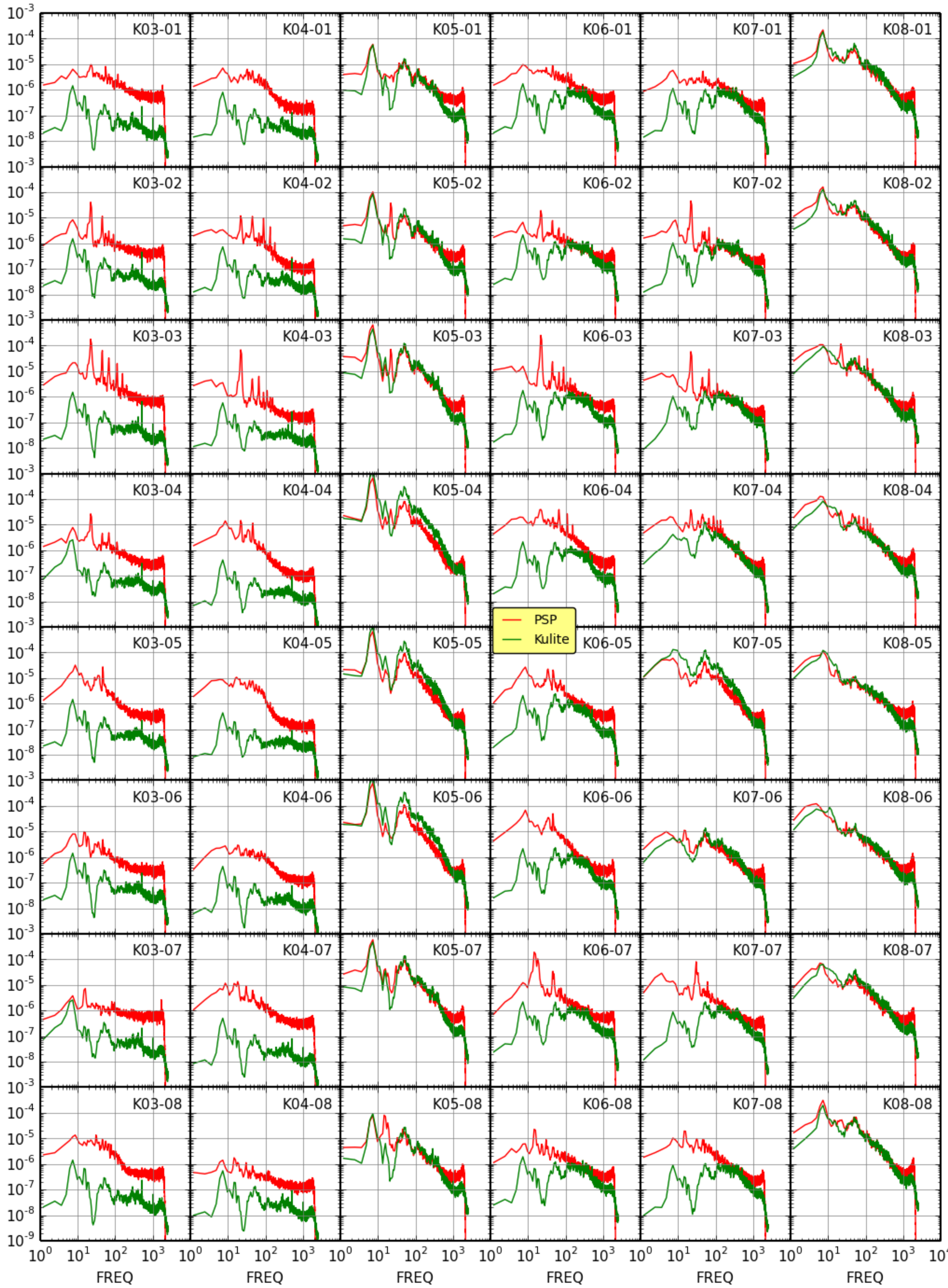

a. Stations 3 through 8.
Figure 6. PSD (psi^2/Hz) comparison, Mach 0.85 Alpha -4 deg.

Approved for public release; distribution is unlimited.

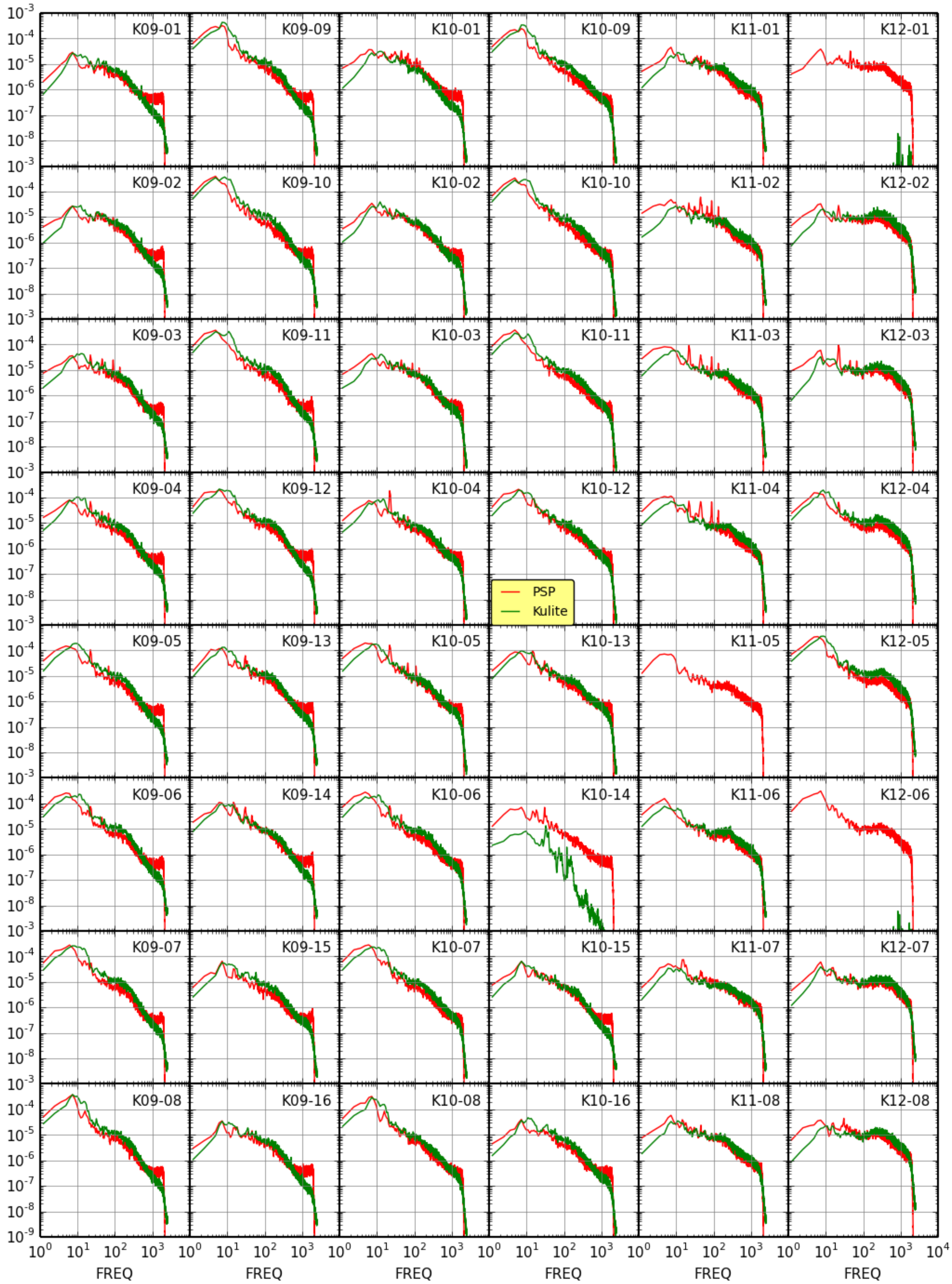

b. Stations 9 through 12.
Figure 6. Continued.

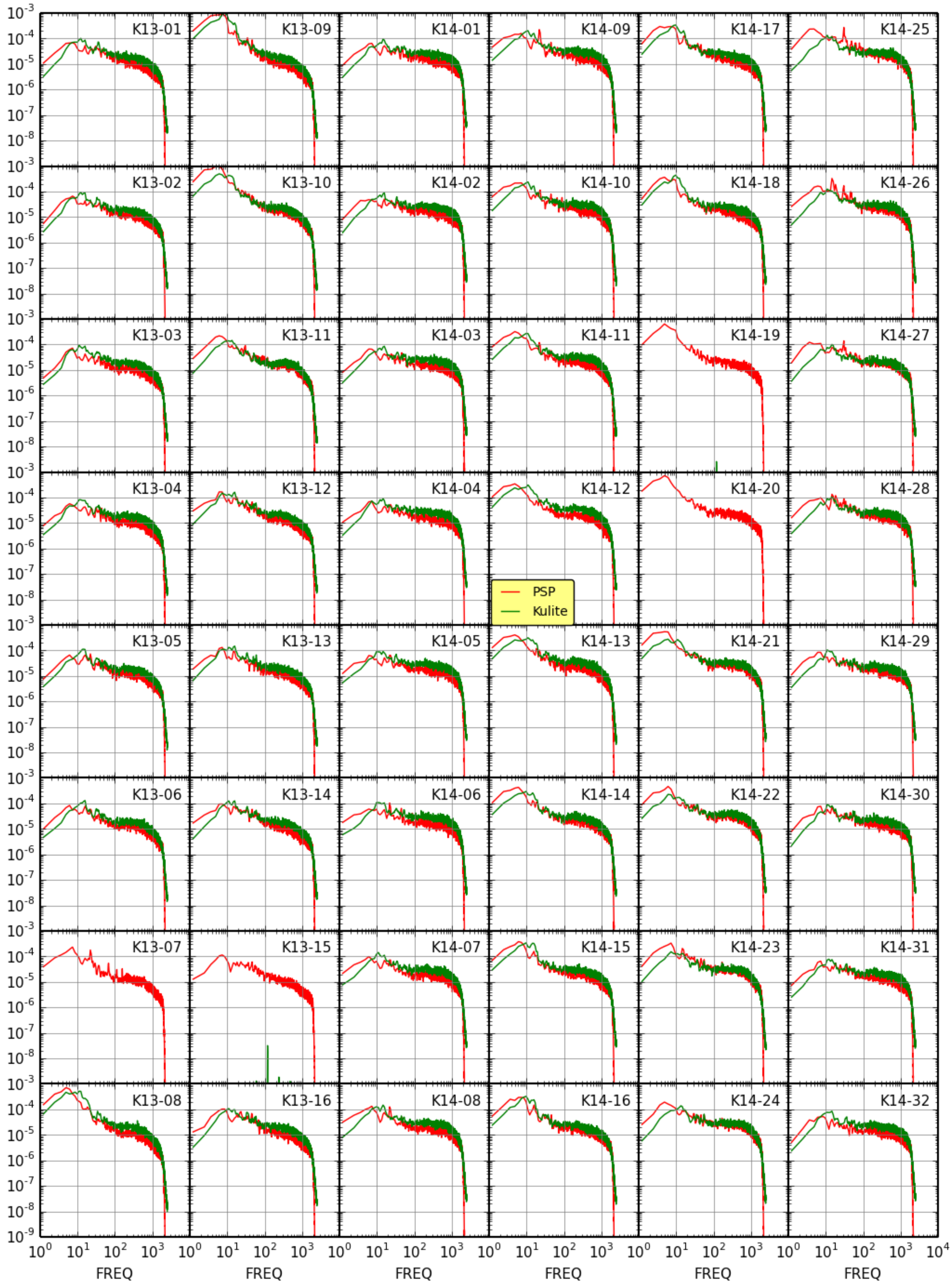

c. Stations 13 through 14.
Figure 6. Continued.

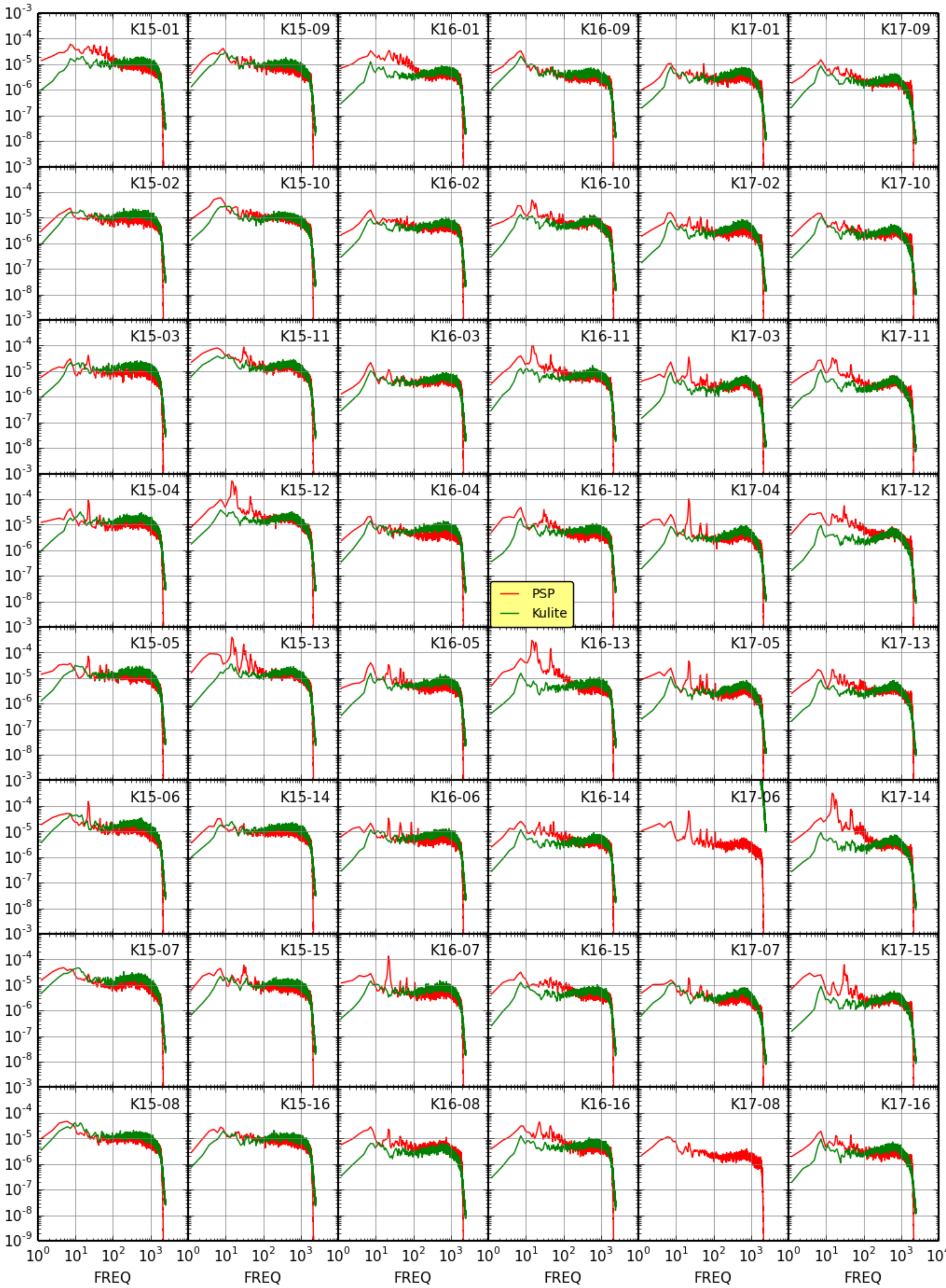

d. Stations 15 through 17.
Figure 6. Concluded.

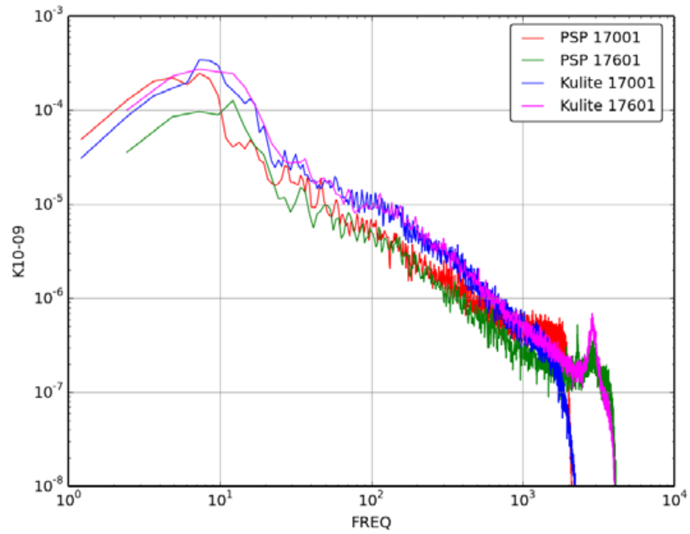

Figure 7. Comparison of 5 kHz (17001) and 10 kHz rate (17601), Mach 0.85, Alpha -4 deg.

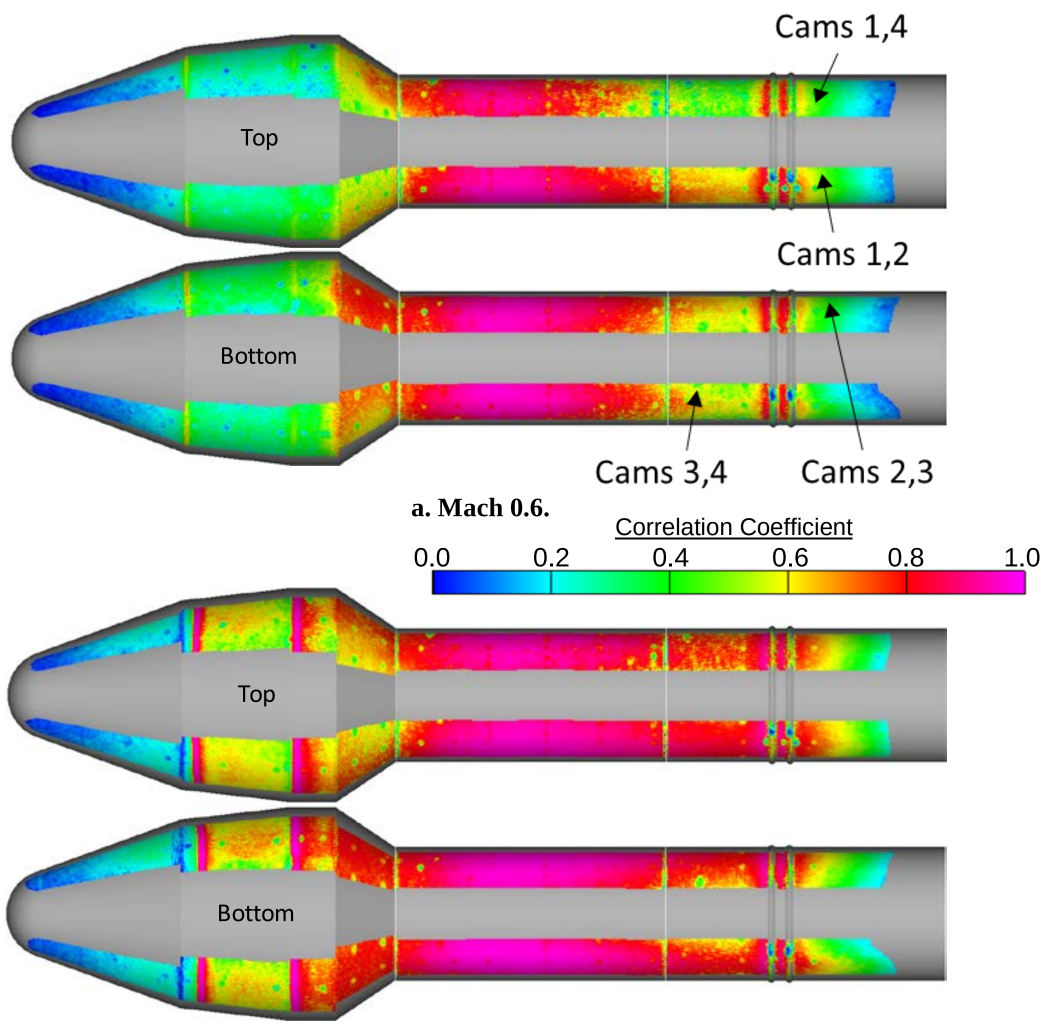

a. Mach 0.6.

b. Mach 0.8.

Figure 8. Correlation Coefficient between Cameras, Alpha -4 deg.

Approved for public release; distribution is unlimited.

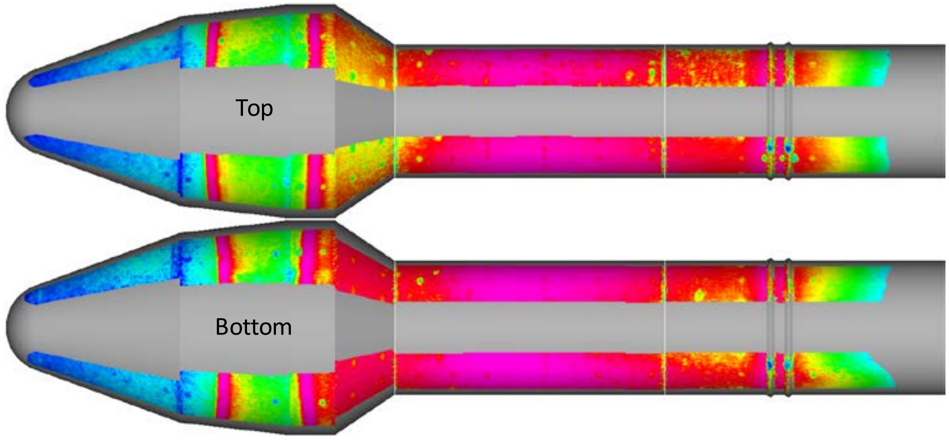

c. Mach 0.85.

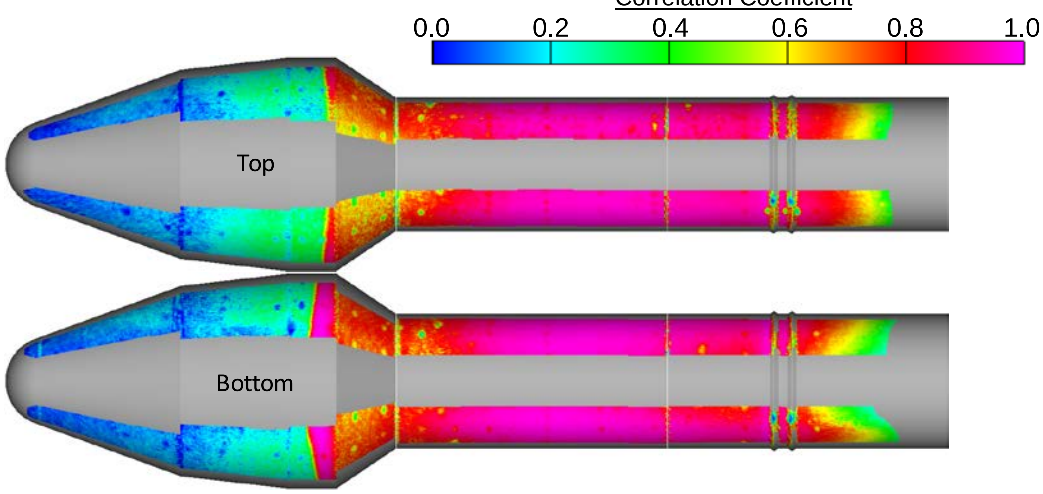

d. Mach 0.92.

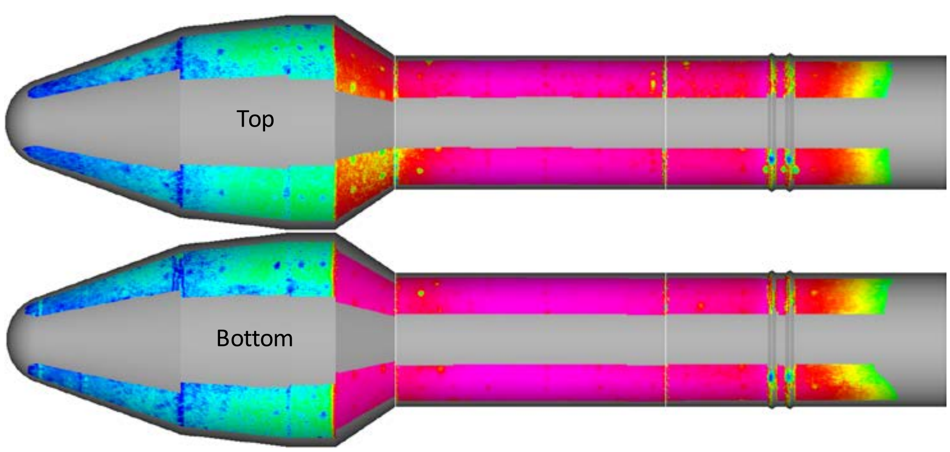

e. Mach 1.025.
Figure 8. Continued.

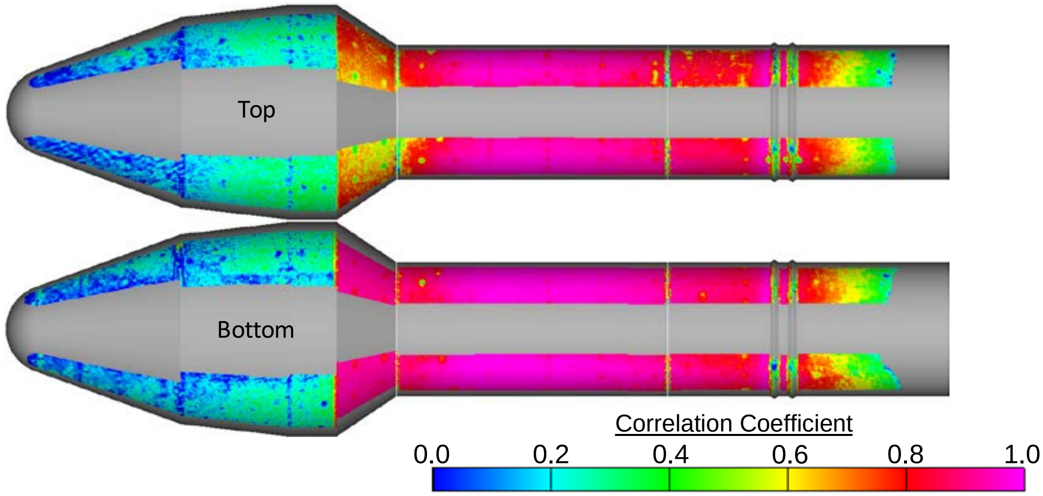

f. Mach 1.1.
Figure 8. Concluded.

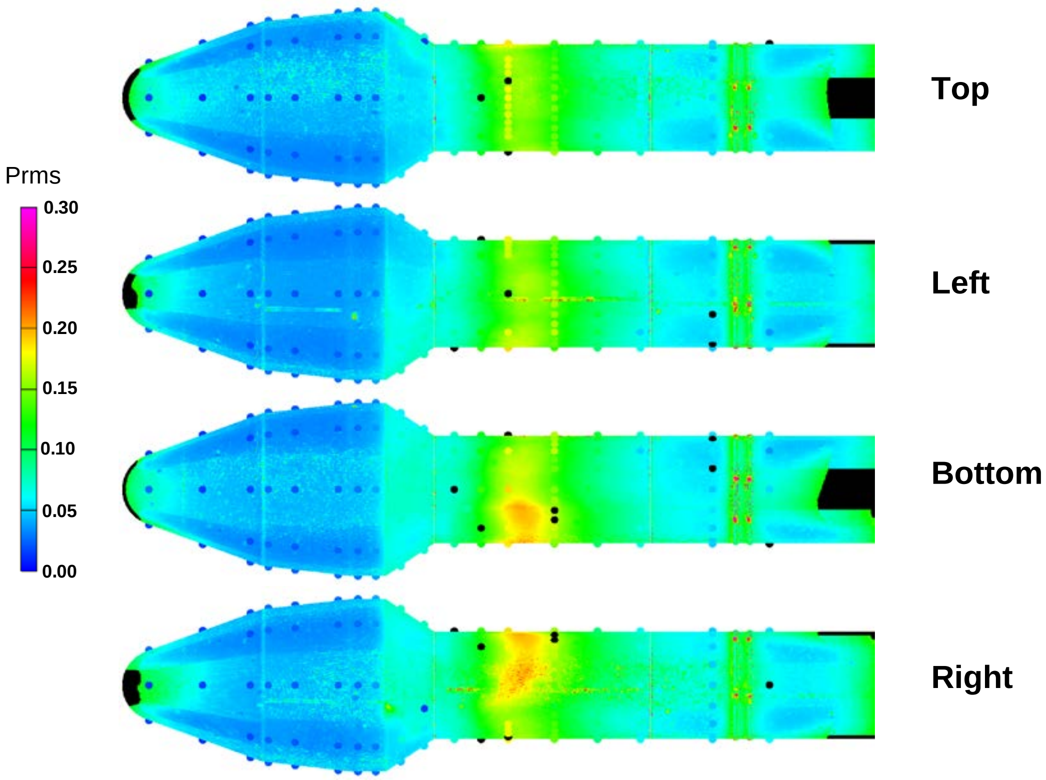

a. Mach 0.6.
Figure 9. RMS distribution, psi, Alpha -4 deg.

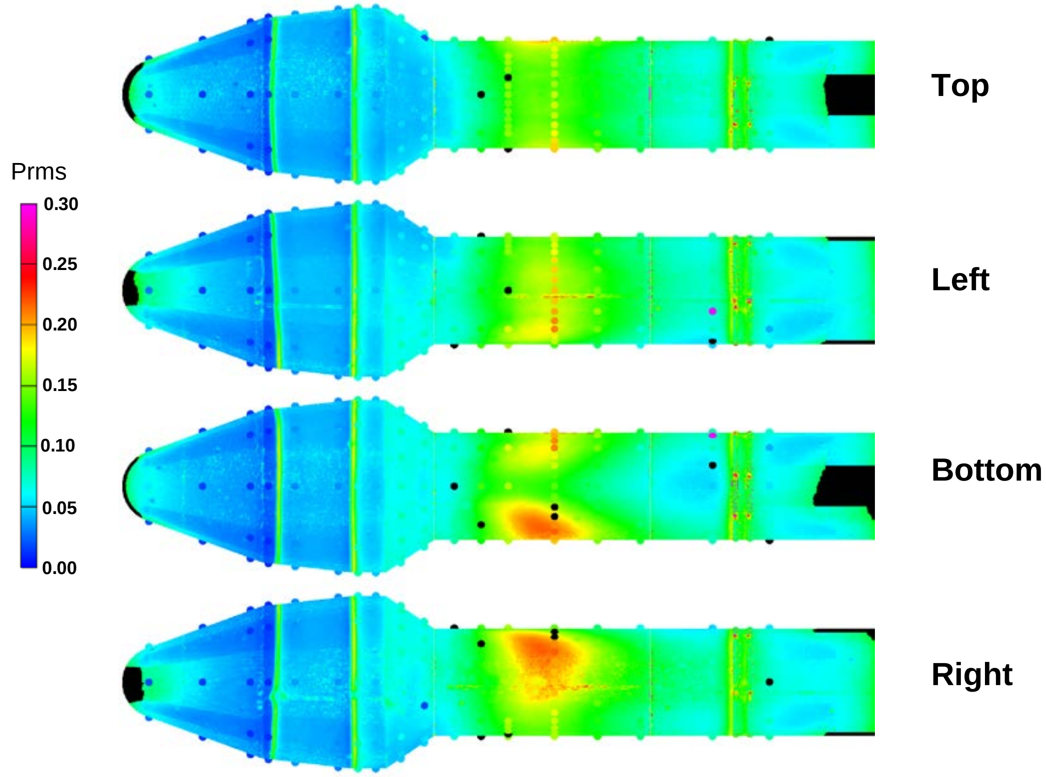

b. Mach 0.8.

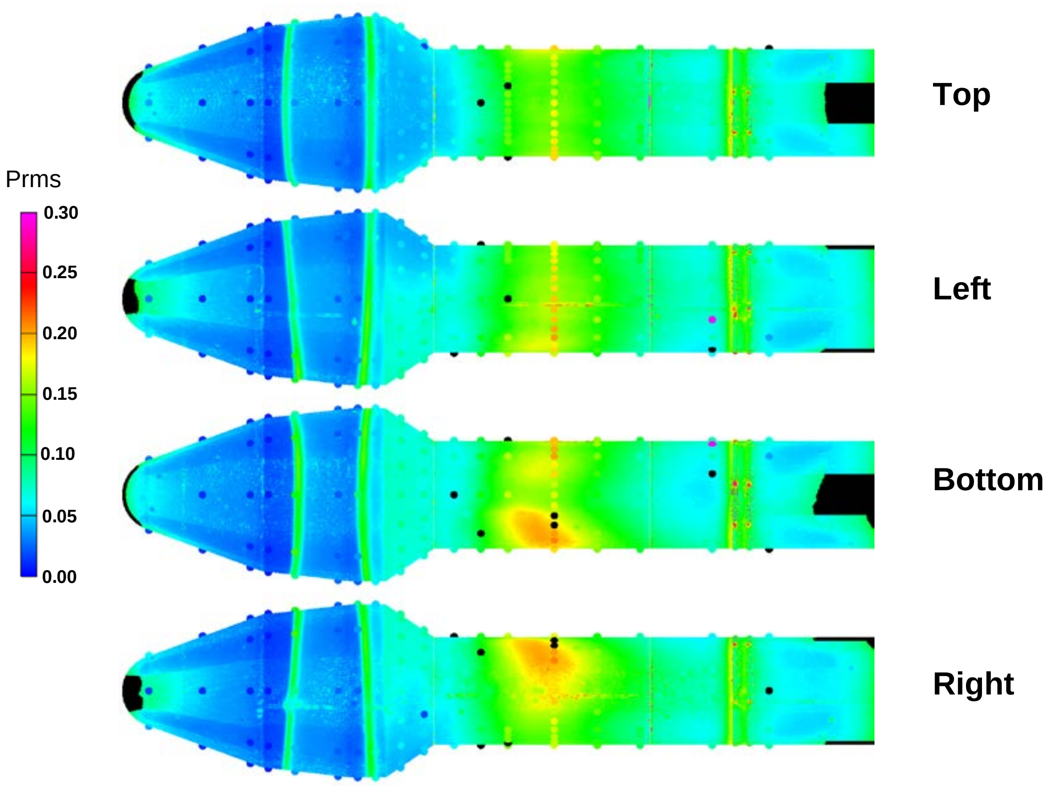

c. Mach 0.85.
Figure 9. Continued.

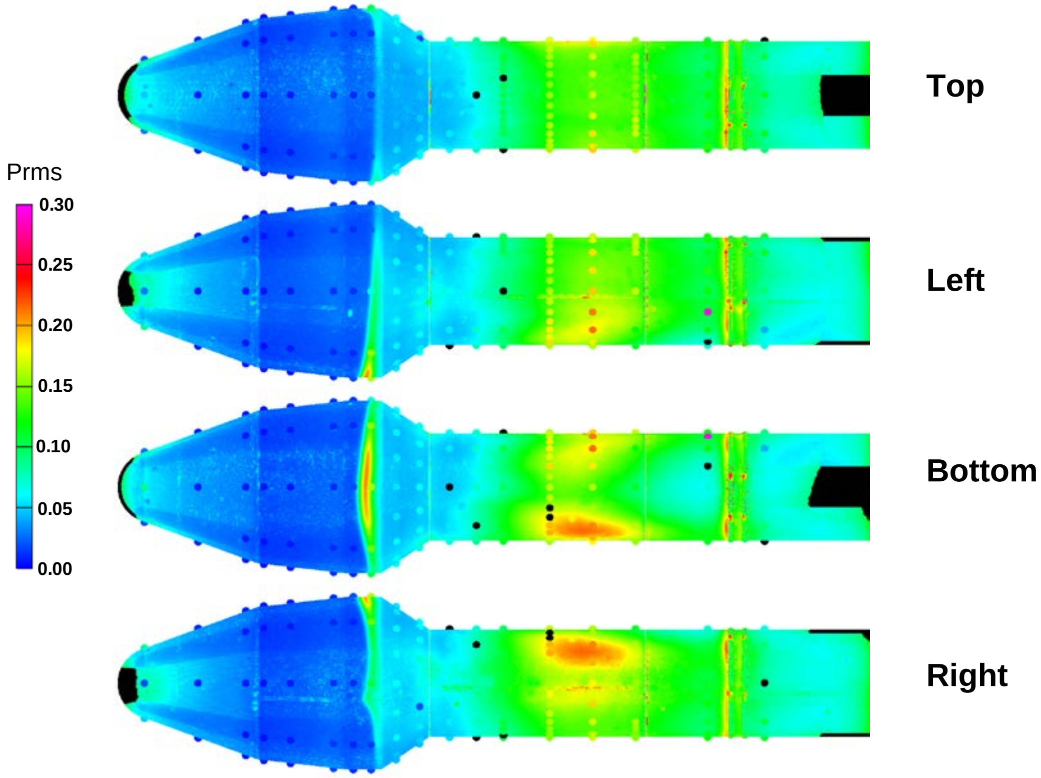

d. Mach 0.92.

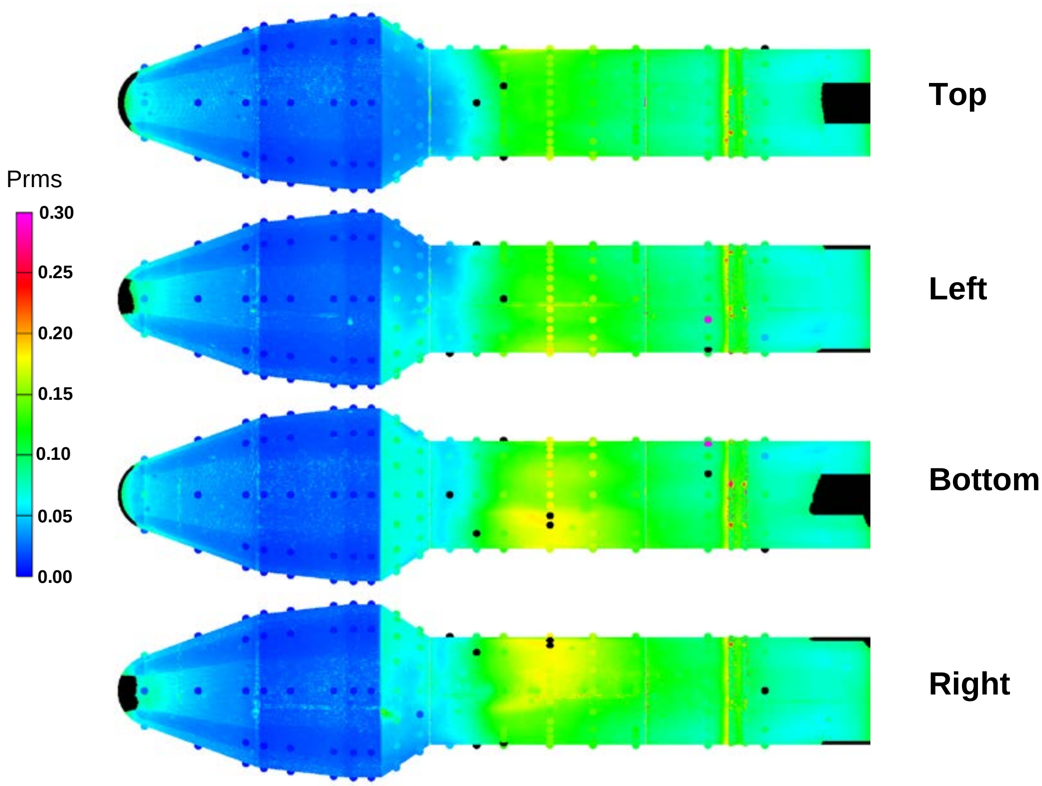

e. Mach 1.025.
Figure 9. Continued.

Approved for public release; distribution is unlimited.

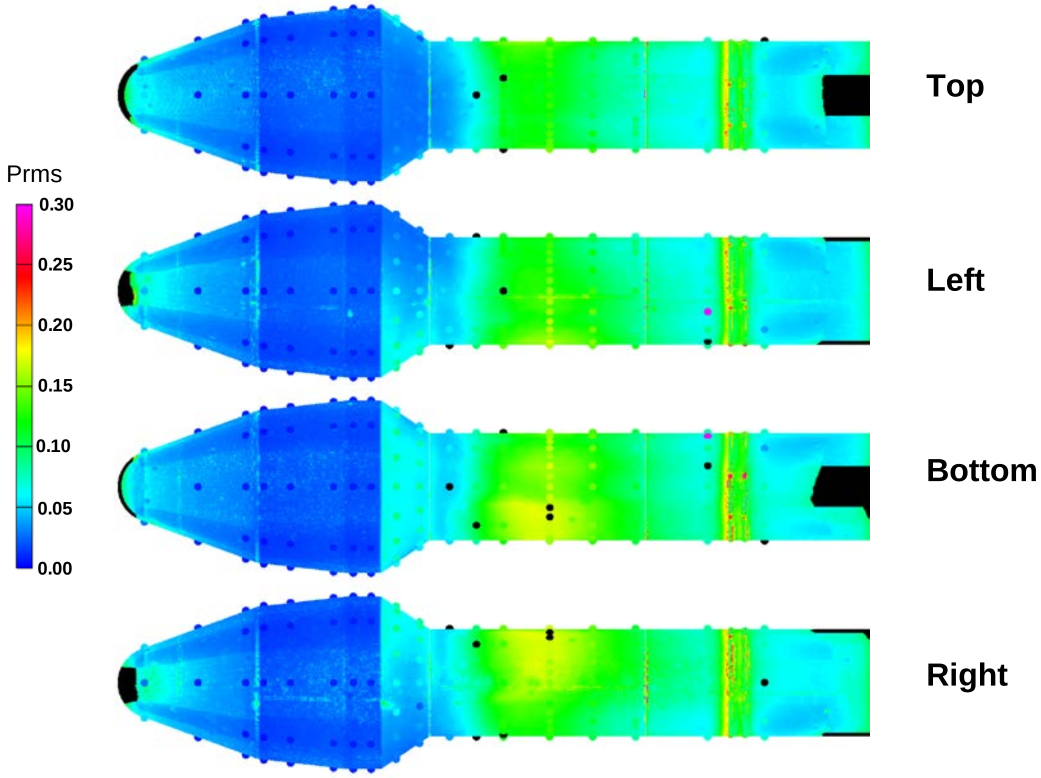

f. Mach 1.1.
Figure 9. Concluded.

B. Full Surface Sound Pressure Level Distributions

One of the advantages of PSP over point source measurements is the ability to acquire high spatial resolution data over the test article surface. Presenting the vast information available from uPSP in a document is difficult. However, a sample of the SPL distributions for a sequence of frequencies at one of the conditions discussed in the previous section is presented to demonstrate the capability.

The uPSP SPL distribution on the lower half of the model for the first 60 frequencies are presented in Fig. 10 for Mach 0.85 and Alpha -4 deg. The standing shocks are fluctuating at a frequency of 6-7 Hz with secondary peaks around 50Hz and the sharp boundaries of this energy content are visible. The sparse transducer distribution is not capable of identifying the width of these narrow bands and could possibly miss detecting the signal completely (see bubbles in Fig. 9c Top). The separation on the boattail has the highest energy over frequencies from 2-10 Hz and the reattachment on the second stage occurs over a much broader range. The dual lobes of the reattachment are also visible. The high SPL data on the flanges (the red areas) are image processing artifacts where the flange attachment screws were located and paint was missing.

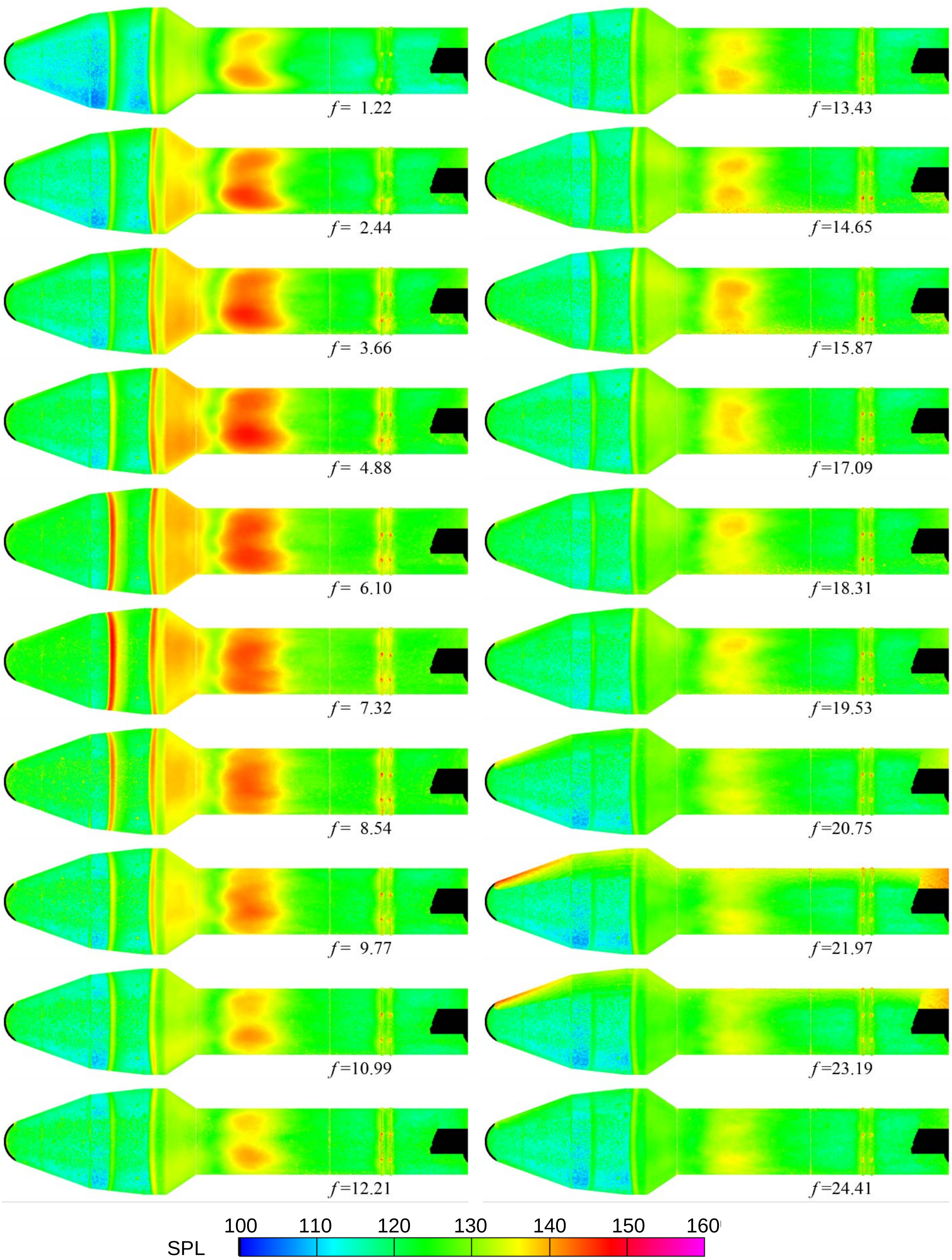

Figure 10. SPL distribution, dB, Mach 0.85, Alpha -4 deg.

Approved for public release; distribution is unlimited.

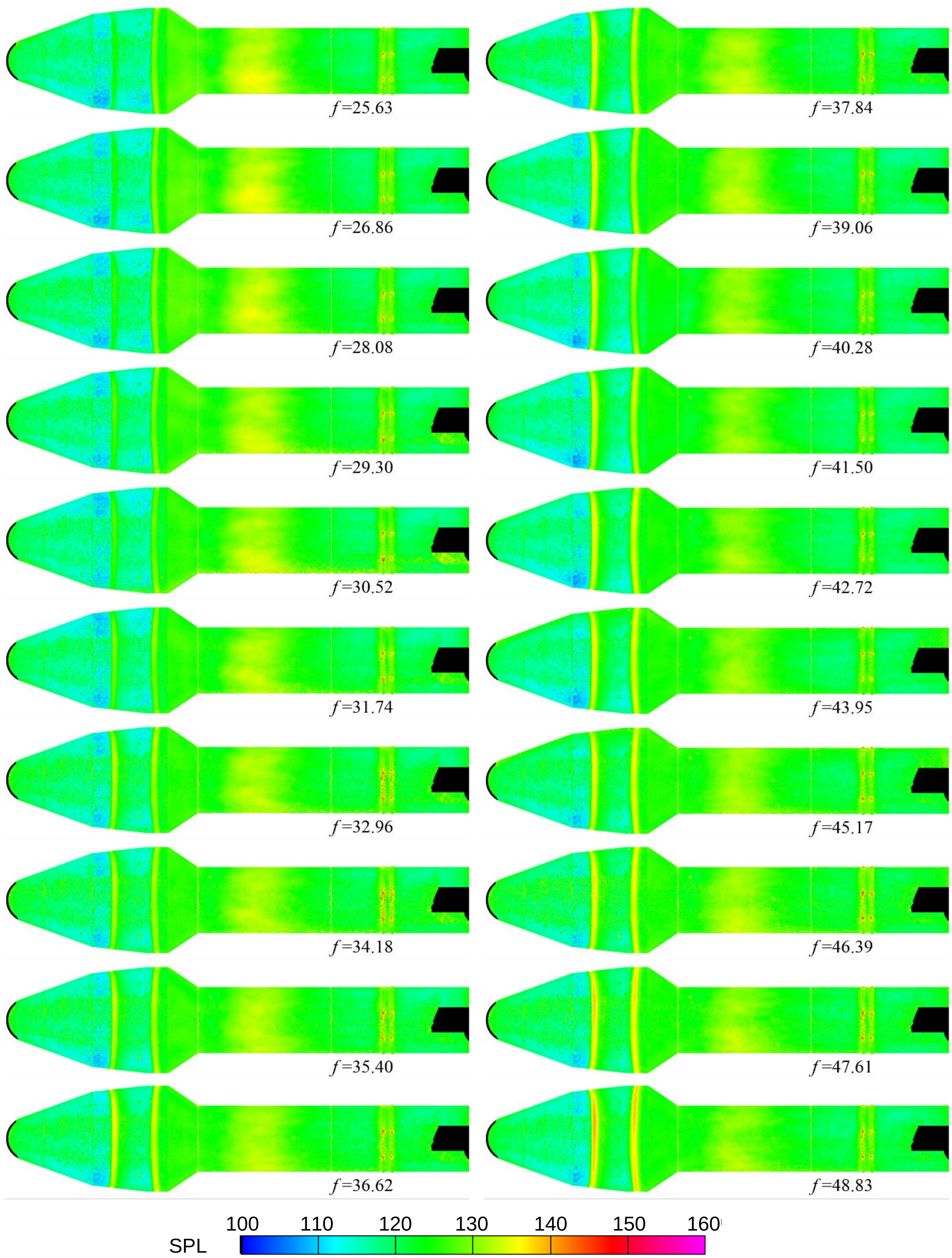

Figure 10. Continued.

Figure 10. Concluded.

C. Fluctuating Integrated Loads

The uPSP and Kulites pressure/time history data were integrated to produce fluctuating-load/time history data on which PSD and RMS calculations were made. The PSDs for Mach 0.6 and 0.85 at Alpha -4 deg are presented in Fig. 11. As mentioned earlier, the camera 2 movement introduced a false 22 Hz pressure fluctuation peak which now propagates into the integrated side-force data. The 22 Hz peak and harmonics are most evident in the uPSP side force at stations 1.5 through 13.17 and 26.57 through 36.17 where the aerodynamic energy content is small. Also present are peaks at the drive system generated frequencies for the two test conditions when aerodynamic energy content is small. The energy levels for the first three stations have good agreement (at least over a portion of the frequency range). Recall from Fig. 5, the uPSP PSD levels at the transducer locations were typically more than the Kulite levels because the PSP was noise limited. However, the integration of uncorrelated noise should cancel out resulting in no added force. There is a significant difference at the remaining stations in Fig. 11 with the Kulite loads consistently higher than the uPSP loads as a result of the conservative load estimation.

One of the most important products from a buffet test is the line load distribution along the vehicle. The BFF methodology applies coherence corrections to the Kulite loads in an attempt to account for the sparse instrumentation. A simplified integration methodology that assumed full coherence to the mid-point between sensors (azimuthally) was used for this paper. The line loads (force per unit length) were computed as RMS of the time fluctuating loads from the uPSP data at 77 stations and from the Kulite data at the 18 transducer stations. In addition, line loads were computed using the uPSP values only at the Kulite locations for direct comparison of data from the two sources to evaluate the simplified integration methodology. A comparison of line loads from the continuous uPSP data and the discrete Kulite data and uPSP data at the Kulite locations is presented in Fig. 12. The loads from the Kulites and uPSP at the Kulite locations compare favorably from Sta. 9.67 to 36.17. These are regions where the uPSP values are significant and above the noise floor. However, at Sta. 1.5 through 8.17 the discrete uPSP loads are significantly larger as a result of the noise dominated source. By spreading the uPSP point source values azimuthally around the model, the noise becomes correlated and does not cancel out. Interestingly, the Kulite and continuous uPSP loads at these stations match very well because the data in this region has little azimuthal variation and the uncorrelated uPSP noise cancels. Conversely, the rest of the model has significant azimuthal variation which results in the discrete loads being significantly larger than the continuous uPSP.

The BFF methodology uses a coherence value of 0.5 or greater to determine the distance over which a transducer value is valid to be applied. The coherence of the uPSP data at the transducer locations to surrounding uPSP data, for longitudinal cut lines at 180 and 225 deg radial angle, was computed in the stream-wise and radial directions and is presented as composite illustrations in Fig. 13. The black lines indicate the longitudinal boundaries over which coherence was computed for each station. The condition presented is for Mach 0.92 and Alpha -4 deg to illustrate the coherence elongation in the azimuthal direction at Sta. K08, where a strong shock is present (see Fig. 9d), and elongation in the stream-wise direction for structures that are propagating downstream on the second stage. The majority of the instrumentation spacing exceed the coherence criteria which will result in conservative (excessive) load estimates.

Comparisons of the line loads at each test condition for the 2 flange configuration are presented in Fig. 14. Several things are worth noting in the data. One is the trend for Alpha 0 deg where Kulite and uPSP data are consistently together above or below the data at ±Alpha. Second is the repeatability of both data sources at ±Alpha for most conditions with a symmetric model. Third is the detail of the load distribution from the uPSP which has peaks that are missed by the sparse transducer instrumentation. The first two trends are good justification for the validity of the uPSP technique and the results prove what was always thought, that the sparse instrumentation resulted in conservative loads. As with steady-state PSP, the complete surface coverage overcomes the limitation of the point source accuracy when the goal is integrated pressure loads (steady or fluctuating).

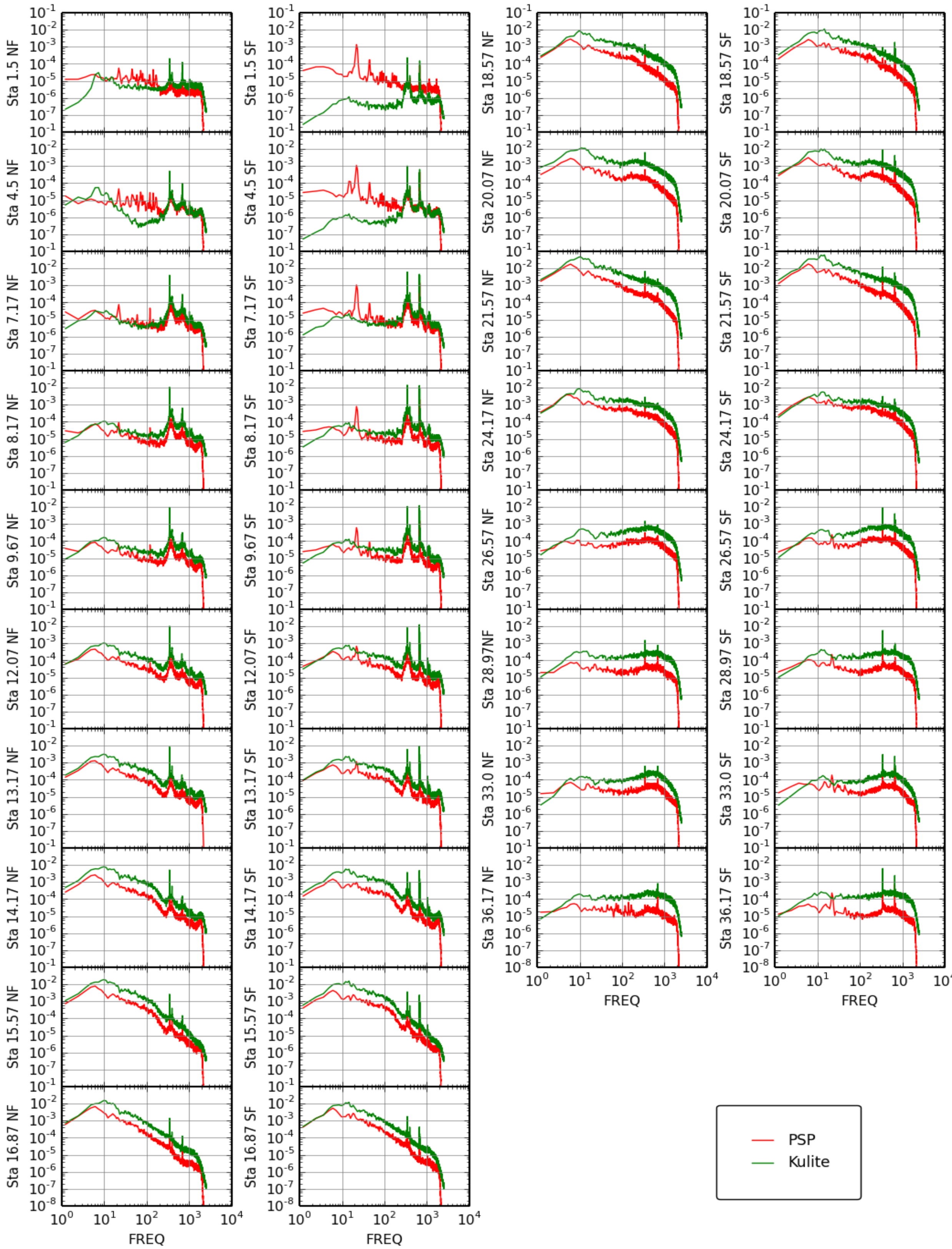

a. Mach 0.6.
Figure 11. PSD ((lb/in.)^2/Hz) comparison, Alpha -4 deg.

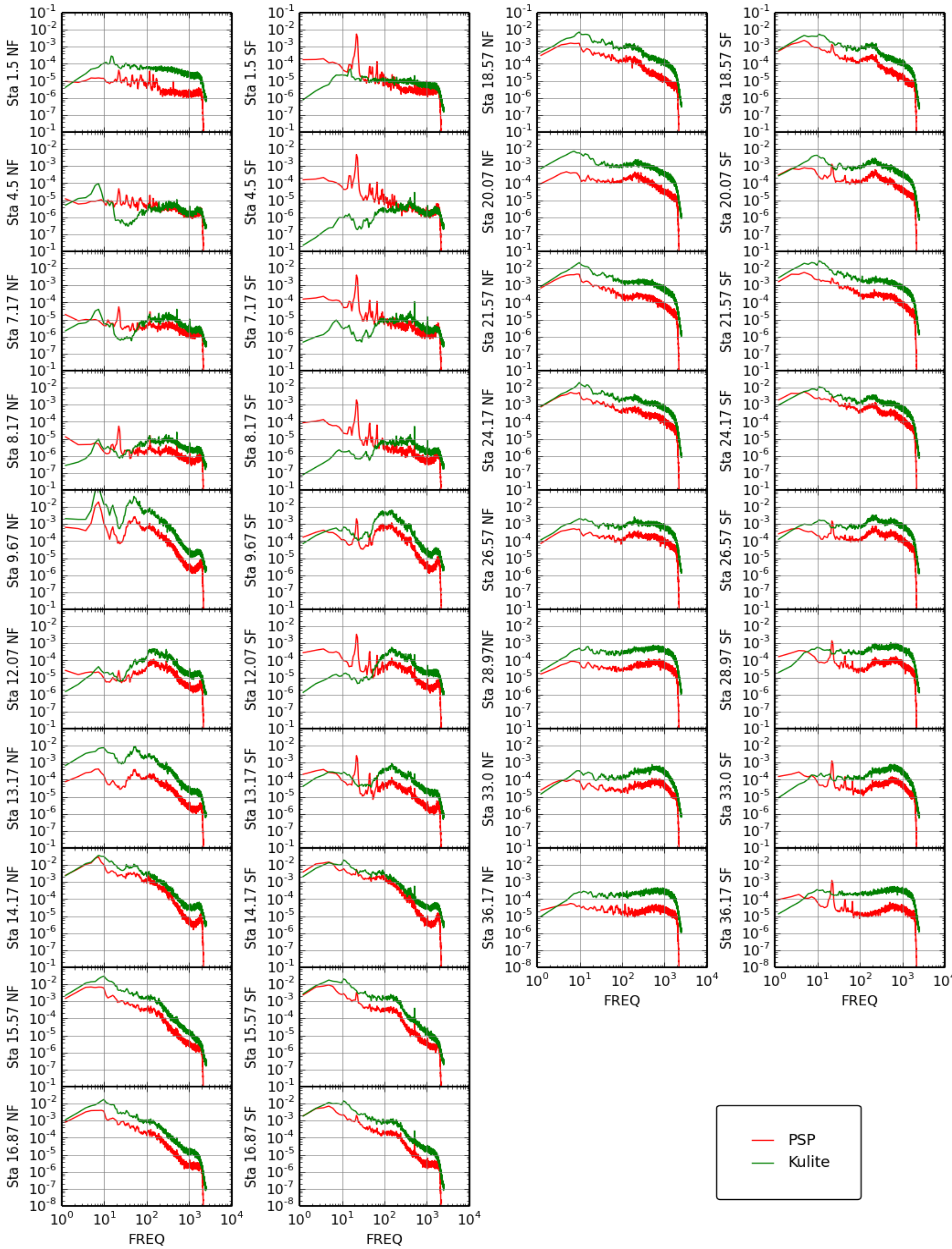

b. Mach 0.85.
Figure 11. Concluded.

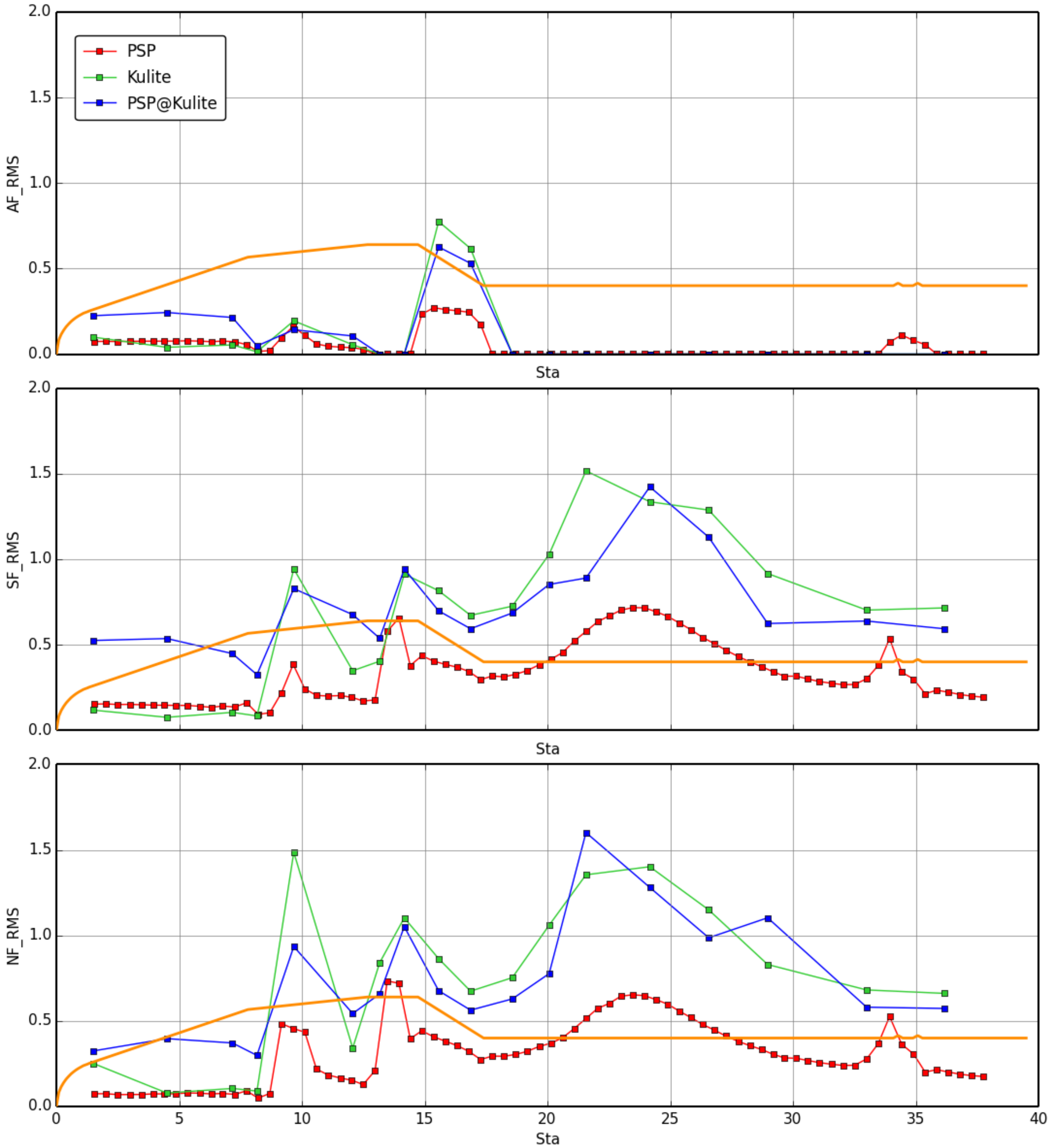

Figure 12. Data source line load comparisons, lb/in., Mach 0.85 and Alpha -4 deg.

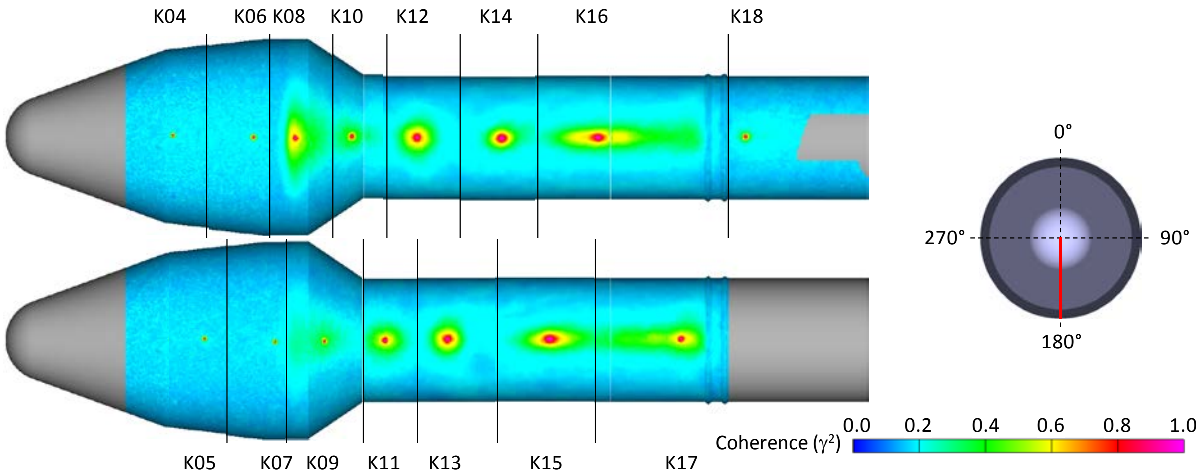

a. Radial 180 deg.

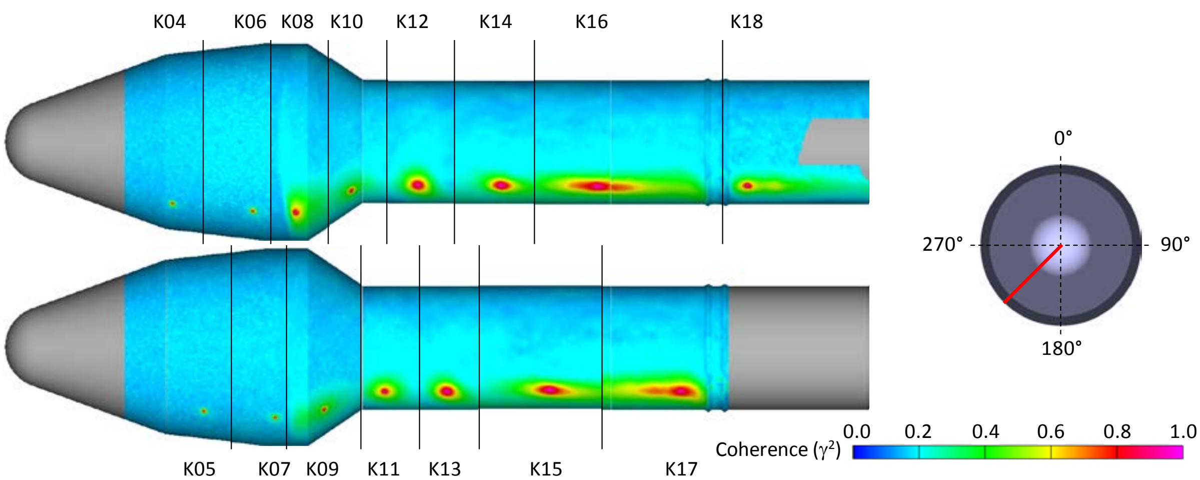

b. Radial 225 deg.
Figure 13. Composite coherence distribution, Mach 0.92, Alpha -4 deg.

Approved for public release; distribution is unlimited.

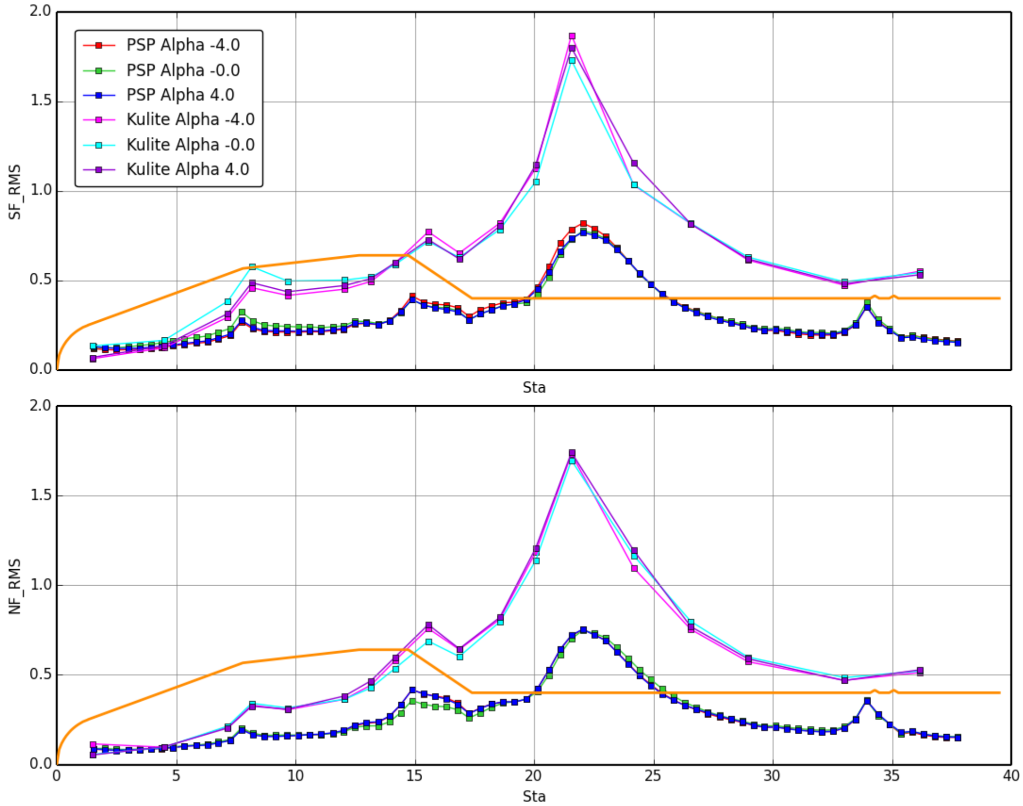

a. Mach 0.6.

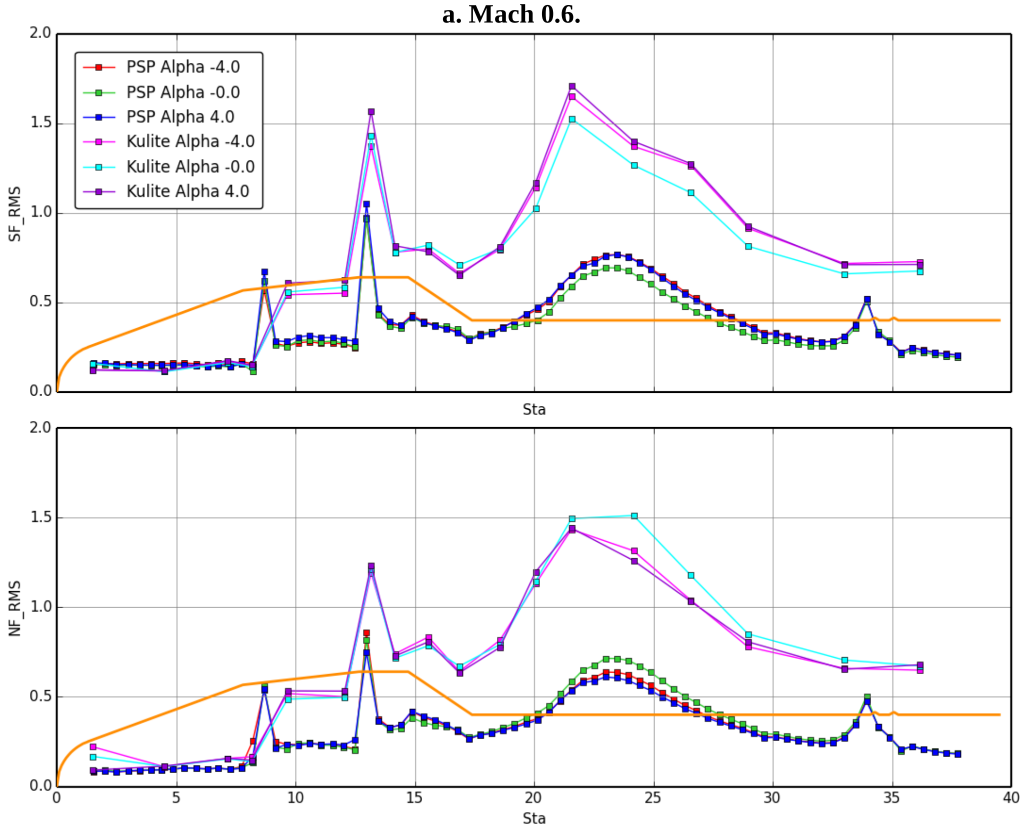

b. Mach 0.8.

Figure 14. Line load comparison, lb/in.

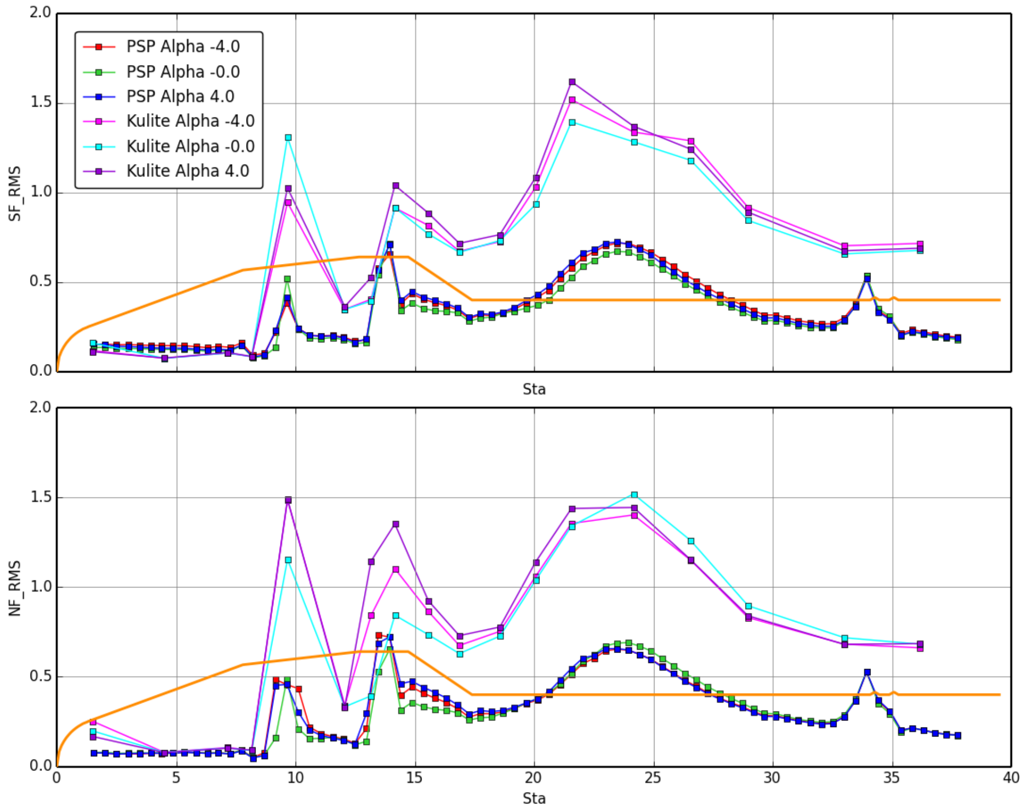

c. Mach 0.85.

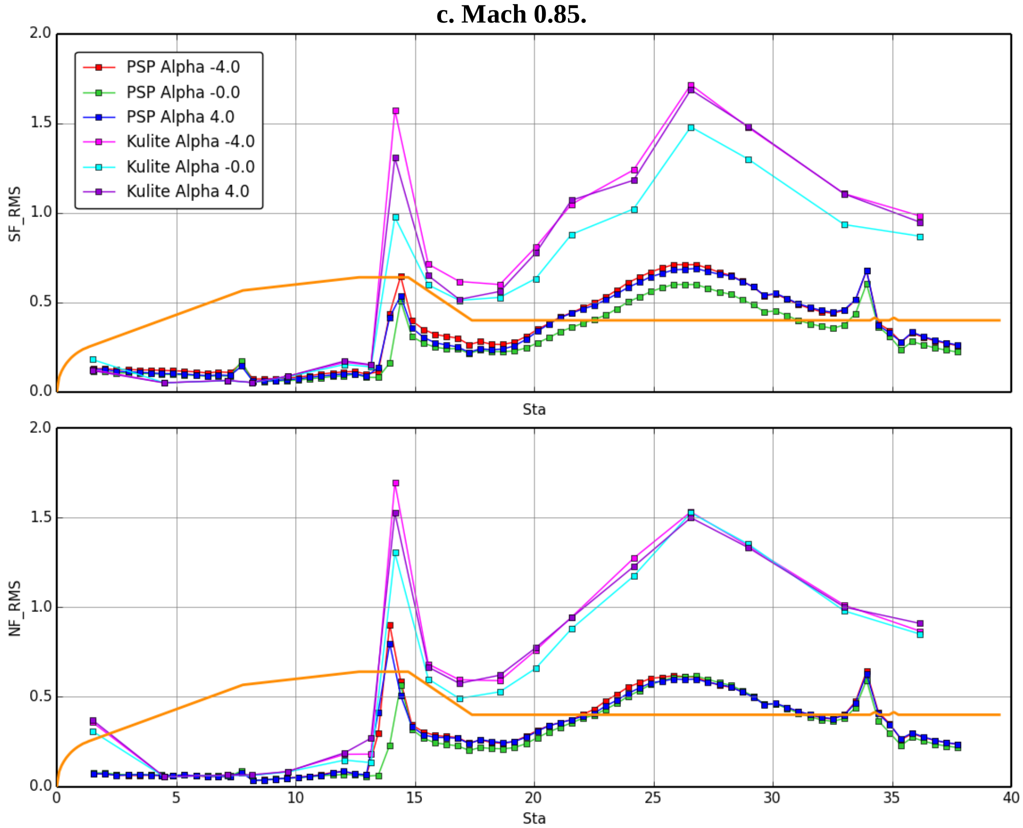

d. Mach 0.92.

Figure 14. Continued.

Approved for public release; distribution is unlimited.

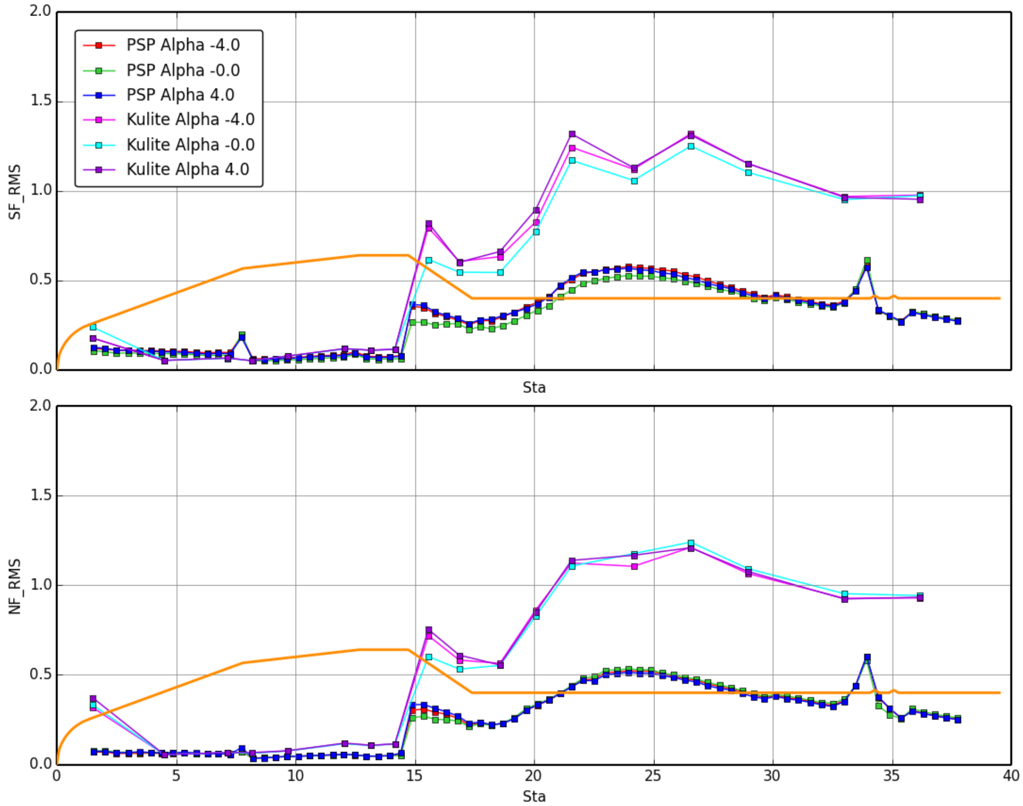

e. Mach 1.025.

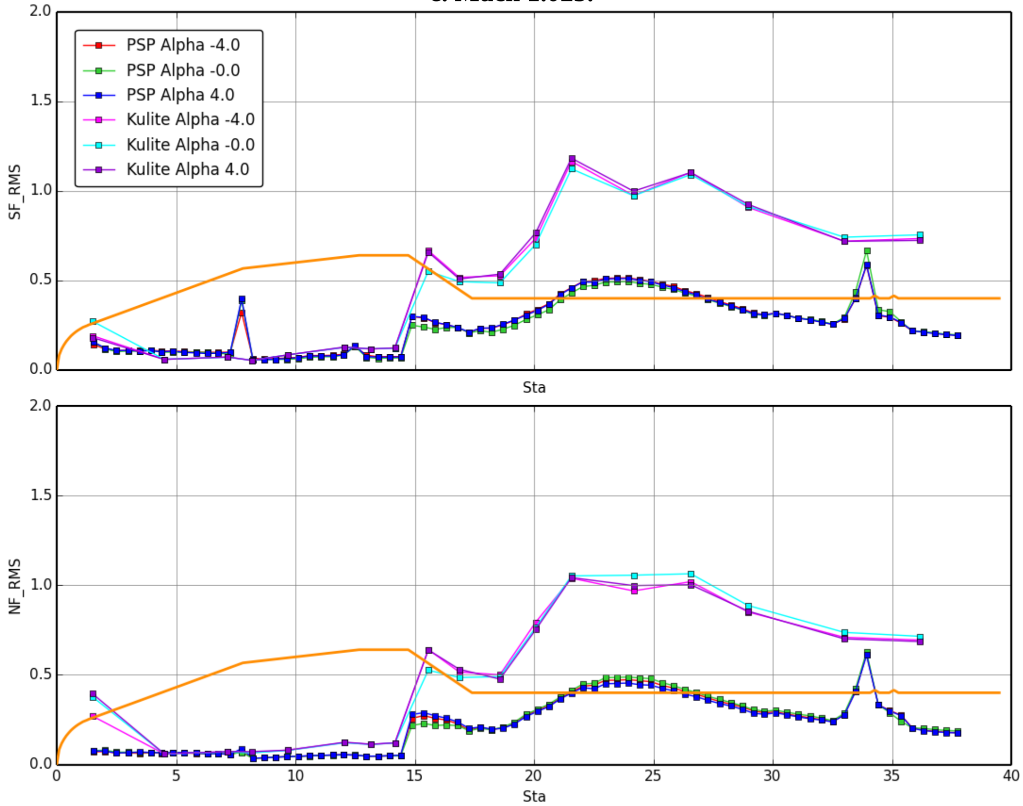

f. Mach 1.1.

Figure 14. Concluded.

V. Summary

The use of unsteady PSP on a generic launch vehicle was demonstrated in the NASA Ames 11- by 11-Foot Transonic Wind Tunnel. The uPSP data were compared to and validated against results from unsteady pressure transducers installed in the model. Some conclusions and observations from the test are as follows:

- The power spectral density content from the uPSP compared well with the unsteady pressure transducer data when the pressure fluctuations were above the uPSP noise floor. The strong peak frequencies matched extremely well between the two sources of data. Unfortunately, one of the high speed cameras was not mounted securely enough and vibrated at a frequency near 22 Hz which resulted in perceived pressure fluctuations from that camera. Also, energy content from the tunnel around 3000 Hz folded over into the 5 kHz PSP data and required filtering (a significant time addition to image processing) to reduce the aliasing. In hindsight, the majority of the test should have been recorded at 10 kHz as the few runs acquired at this rate agreed better with the Kulite data.

- The frames must be synchronized to combine data from the four high-speed cameras. Analysis of correlation between cameras in overlap regions proved the cameras were synchronized. In addition, the correlations provided insight into the noise limited regions of the uPSP data and why better agreement occurred when correlation was near 1.

- The RMS distribution of the uPSP data provided detailed information over the vehicle surface identifying narrow bands of energy where the standing shocks were oscillating. The uPSP RMS values were larger than the Kulite data on the nose of the payload as expected since the uPSP was dominated by noise. The RMS comparison was very good between the uPSP and the Kulites over the boattail and second stage and on the nose when shocks were present.

- One of the advantages of PSP over point source measurements is the ability to acquire high spatial resolution data. The SPL distribution provided insight into spectral content in a way that is not possible from XY plots. The uPSP data is the equivalent of ~350,000 Kulites distributed over the model surface.

- The coherence distances computed from the continuous uPSP data illustrate the limited range over which the discrete Kulite data are valid, based on a coherence value of 0.5. The majority of the instrumentation spacing exceeds the coherence criteria.

- The most important result from the test was the line loads generated from the uPSP. The uPSP loads were validated by comparison with the Kulite loads using the discrete data from the two sources. However, the continuous uPSP loads provided a more accurate measurement and detail than is possible with discrete measurements. As expected, the sparse instrumentation resulted in conservative loads.

The results of the test demonstrate the ability to determine more accurate buffet forcing functions using unsteady PSP than is possible with sparse point source instrumentation.

Acknowledgments

The authors would like to thank Dr. Wim Ruyten of Euclidian Optics, Inc. for developing new image processing capabilities required for this test. Also, thanks to Zach Lowry, private consultant, for developing new data acquisition software and improvment of 10 Gb communcation for the high-speed cameras. Special thanks to Dr. David Schuster of the NASA Engineering and Safety Center for his enthusiastic support of this project.

References

[1]Sellers, M. E. and Brill, J. A. "Demonstration of a Pressure Sensitive Paint in the AEDC 16-ft Transonic Wind Tunnel Using the TST Model." AIAA Paper 94-2481, 18th AIAA Aerospace Ground Testing Conference, Colorado Springs, CO, June 1994.

[2]Sellers, M. E. "Demonstrations of a Pressure Sensitive Paint Data System in the AEDC Propulsion Wind Tunnel 16T." AEDC-TR-95-8, October 1995.

[3]Sellers, M. E. "Demonstration Comparison of an AEDC and a Russian Developed Pressure Sensitive Paint in the AEDC Propulsion Wind Tunnel 16T." AEDC-TR-95-88, December 1995.

[4]Sellers, M. E. "Pressure Sensitive Paint Data on the Transonic Technology Wing Demonstrator (TST) in the AEDC Propulsion Wind Tunnel 16T." AEDC-TR-98-3, June 1998.

[5]Sellers, M. E. "Application of Pressure Sensitive Paint for Determining Aerodynamic Loads on a Scale Model of the F-16C." AIAA Paper 2000-2528, 21st AIAA Aerodynamic Measurement Technology and Ground Testing Conference, Denver, CO, June 2000.

[6]Sellers, M. E. "Advances in AEDC's Lifetime Pressure-Sensitive Paint Program." AIAA Paper 2005-7638, U.S. Air Force T&E Days, Nashville, TN, December 2005.

[7]Sellers, M. E. "AEDC's Portable Pressure-Sensitive Paint Data Acquisition System." AIAA Paper 2007-1606, U.S. Air Force T&E Days, Destin, FL, February 2007.

[8]Sellers, M. E. "Validation of Integrated Panel Loads on a Fighter Aircraft Model Using Pressure-Sensitive Paint at AEDC." AEDC-TMR-08-T2, January 2008.

[9]Sellers, M. E. "Pressure-Sensitive Paint Data on the Facility Aerodynamics Validation and Research (FAVOR) Model at AEDC." AEDC-TR-09-F-34, December 2009.

[10]Sellers, M. E. "Demonstration of a Temperature-Compensated Pressure Sensitive Paint on the Orion Launch Abort Vehicle." AIAA Paper 2011-3166, 29th AIAA Applied Aerodynamics Conference, Honolulu, HI, June 2011.

[11]Sellers, M. E. and Nelson, M. A. "Dynamic Pressure-Sensitive Paint Demonstration in AEDC Propulsion Wind Tunnel 16T." AIAA Paper 2016-1146, AIAA Science and Technology Forum and Exposition (SciTech 2016), San Diego, CA, June 2016.

[12]Coe, C. F. and Nute, J. B. "Steady and Fluctuating Pressures at Transonic Speeds on Hammerhead Launch Vehicles." NASA TM X-778, 1962.

[13]Flaherty, W., Reedy, T. M., Elliot, G. S., Austin, J. M., Schmit, R. F., and Crafton, J., "Investigation of Cavity Flow Using Fast-Response Pressure Sensitive Paint," AIAA Paper 2013-0678, 51st AIAA Aerospace Sciences Meeting, Grapevine, TX, January 2015.

[14]Gregory, J. W., Asai, K., Kameda, M., Liu, T., and Sullivan, J. P. "A Review of Pressure-Sensitive Paint for High Speed and Unsteady Aerodynamics," Proceedings of the Institution of Mechanical Engineers, Part G, *Journal of Aerospace Engineering*, Vol. 222, No. 2, pp. 249-290, (2008).

[15]Schlichting, H., *Boundary Layer Theory*. McGraw-Hill, New York, 1979 (Seventh Edition).

[16]Bores Signal Processing "FFT window functions", www.bores.com